



HAL
open science

The role of evaporites in the formation of gems during metamorphism of carbonate platforms: a review

Gaston Guiliani, Jean Dubessy, Daniel Ohnenstetter, David Banks, Yannick Branquet, Julien Feneyrol, Anthony E. Fallick, Jean-Emmanuel Martelat

► To cite this version:

Gaston Guiliani, Jean Dubessy, Daniel Ohnenstetter, David Banks, Yannick Branquet, et al.. The role of evaporites in the formation of gems during metamorphism of carbonate platforms: a review. *Mineralium Deposita*, 2018, 53 (1), pp.1-20. 10.1007/s00126-017-0738-4 . insu-01528349

HAL Id: insu-01528349

<https://insu.hal.science/insu-01528349v1>

Submitted on 28 Nov 2019

HAL is a multi-disciplinary open access archive for the deposit and dissemination of scientific research documents, whether they are published or not. The documents may come from teaching and research institutions in France or abroad, or from public or private research centers.

L'archive ouverte pluridisciplinaire **HAL**, est destinée au dépôt et à la diffusion de documents scientifiques de niveau recherche, publiés ou non, émanant des établissements d'enseignement et de recherche français ou étrangers, des laboratoires publics ou privés.

Mineralium Deposita

The role of evaporites in the formation of gems during metamorphism of carbonate platforms: a review --Manuscript Draft--

Manuscript Number:	
Full Title:	The role of evaporites in the formation of gems during metamorphism of carbonate platforms: a review
Article Type:	Regular Articles
Corresponding Author:	Gaston Giuliani, PhD. CRPG/CNRS Vandoeuvre, Meurthe et Moselle FRANCE
Corresponding Author Secondary Information:	
Corresponding Author's Institution:	CRPG/CNRS
Corresponding Author's Secondary Institution:	
First Author:	Gaston Giuliani, PhD.
First Author Secondary Information:	
Order of Authors:	Gaston Giuliani, PhD. jean Dubessy, PhD. Daniel Ohnenstetter, PhD. David Banks, PhD. Yannick Branquet, PhD. Julien Feneyrol, PhD. Anthony Fallick, PhD. Jean-Emmanuel Martelat, PhD.
Order of Authors Secondary Information:	
Funding Information:	Département Soutien et Formation, Institut de Recherche pour le Développement Dr. Gaston Giuliani
Abstract:	<p>The mineral and fluid inclusions trapped by gemstones during the metamorphism of rocks in carbonate platform successions are precious markers for the understanding of the gem genesis. The nature and chemical composition of inclusions highlight the major contribution of evaporites through dissolution or fusion, depending on the temperature of formation from the greenschist to the granulite facies. The fluids are highly saline NaCl-brines circulating either in an open system in the greenschist facies (Colombian and Afghan emeralds) and with huge fluid-rock metasomatic interactions, or sulphurous fluids (ruby, garnet tsavorite, zoisite tanzanite and lapis-lazuli) or molten salts formed in a closed system with a low fluid mobility (ruby in marble) in the conditions of the amphibolite to granulite facies. These chloride-fluoride-sulphate ± carbonate-rich fluids scavenged the metals essential for the gem formation. At high temperature, anions SO₄²⁻, NO₃⁻, BO₃⁻ and F⁻ which are powerful fluxes lowered the temperature of chlorine and fluoride ionic liquids. They provided transport over a very short distance of aluminium, and/or silica and transition metals which are necessary for gem growth. So, the genetic models proposed for these high-value and ornamental gems underline the importance of the metamorphism of evaporites formed on carbonate continental shelves, and emphasises the chemical power accompanying the metamorphism at moderate to high temperatures of these particular evaporite-rich and organic matter-rich protoliths to form gem minerals.</p>
Suggested Reviewers:	Bernd Lehmann, PhD.

Editor Mineralium Deposita, Technical University of Clausthal
lehmann@min.tu-clausthal.de
Dr. Bernd Lehmann, Editor of Mineralium Deposita, who invited us to write this paper on the role of evaporites in the formation of metamorphic gems, published in a short version as "Le fluide, l'Arlésienne du métamorphisme" in the Journal Géochronique, N°136, décembre 2015 entitled "Regards croisés sur le métamorphisme".

Georges beaudoin, PhD.
professor, Université Laval
Georges.Beaudoin@ggl.ulaval.ca
As an Editor of Mineralium Deposita, Journal who invites our group to submit the present ms.
Dr. Beaudoin participated to the bank of PhD. thesis of Julien Feneyrol one of the authors. He knows well the gem thematic

Robert Linnen, PhD.
Professor, Western University
r.linnen@uwo.ca
geochemist specialist of fluids who has experience and knowledge in gems formation

1
2
3
4
5
6
7
8
9
10
11
12
13
14
15
16
17
18
19
20
21
22
23
24
25
26
27
28
29
30
31
32
33

**The role of evaporites in the formation of gems during metamorphism
of carbonate platforms: a review**

Gaston Giuliani^{1,2}, Jean Dubessy³, Daniel Ohnenstetter⁴, David Banks⁵, Yannick Branquet^{6,7},
Julien Feneysel⁸, Anthony E. Fallick⁹, Jean-Emmanuel Martelat¹⁰

1- Université Paul Sabatier, GET/IRD, UMR CNRS-IRD-CNRS 5563, 14 avenue Edouard
Belin, 31400 Toulouse, France

2- Université de Lorraine, CRPG UMR 7358 CNRS-UL, 15 rue Notre-Dame-des-Pauvres,
BP 20, 54501 Vandœuvre-lès-Nancy cedex, France

3- Université de Lorraine, GeoRessources UMR 7359 CNRS-UL, BP 70239, 54506
Vandœuvre-lès-Nancy, France

4- 4 rue Nicolas Chopin, 88130 Marainville-sur-Madon, France

5- University of Leeds, School of Earth and Environment, Woodhouse Lane, Leeds LS2 9JT,
United Kingdom

6- ISTO, UMR 7327-CNRS/Université d'Orléans/BRGM, 1A rue de la Férollerie, 45071
Orléans cedex 2, France

7- Géosciences-Rennes, UMR6881-CNRS/Université de Rennes I, Campus de Beaulieu,
35042 Rennes Cedex, France

8- Arethuse Geology, Latitude Arbois, 1060 Rue René Descartes, 13290 Les Milles, France

9- Isotope Geosciences Unit, S.U.E.R.C., Rankine Avenue, East Kilbride, Glasgow G75
0QF, Scotland, United Kingdom

10- Laboratoire de Géologie de Lyon (LGLTPE), Université de Lyon 1, ENSL, UMR 5276, 2
rue Raphaël Dubois, Géode, 69622 Villeurbanne Cedex, France

34
35
36
37
38
39
40
41
42
43
44
45
46
47
48
49
50
51
52
53
54
55
56
57
58
59
60
61
62
63
64
65
66

Abstract The mineral and fluid inclusions trapped by gemstones during the metamorphism of rocks in carbonate platform successions are precious markers for the understanding of the gem genesis. The nature and chemical composition of inclusions highlight the major contribution of evaporites through dissolution or fusion, depending on the temperature of formation from the greenschist to the granulite facies. The fluids are highly saline NaCl-brines circulating either in an open system in the greenschist facies (Colombian and Afghan emeralds) and with huge fluid-rock metasomatic interactions, or sulphurous fluids (ruby, garnet tsavorite, zoisite tanzanite and lapis-lazuli) or molten salts formed in a closed system with a low fluid mobility (ruby in marble) in the conditions of the amphibolite to granulite facies. These chloride-fluoride-sulphate \pm carbonate-rich fluids scavenged the metals essential for the gem formation. At high temperature, anions SO_4^{2-} , NO_3^- , BO_3^- and F^- which are powerful fluxes lowered the temperature of chlorine and fluoride ionic liquids. They provided transport over a very short distance of aluminium, and/or silica and transition metals which are necessary for gem growth. So, the genetic models proposed for these high-value and ornamental gems underline the importance of the metamorphism of evaporites formed on carbonate continental shelves, and emphasises the chemical power accompanying the metamorphism at moderate to high temperatures of these particular evaporite-rich and organic matter-rich protoliths to form gem minerals.

Keywords

67 gems, emerald, ruby, garnet, zoisite, lapis-lazuli, metamorphism, carbonate platform,
68 evaporites, brines, fingerprints, salinity, molten salts, thermal reduction of sulphates

69 **Introduction**

70 The classical quality-grading criteria for gems are based on clarity, colour, carat and cut.
71 These 4 “C” criteria are dependent on the geological, physical and chemical conditions
72 existing during the gem growth. The formation of coloured gems necessitates the existence of
73 four conditions: (1) a parental fluid issued either from the gem host-rock environment or
74 exotic fluid circulations; (2) a seed surface and sufficient space for the growth of the crystal;
75 (3) the incorporation of trace elements from the parental fluid in the unit cell of the mineral;
76 and (4) the absence of internal crystalline deformation during and after growth.

77 The colour and transparency will make the difference between a mineralogical specimen
78 and a gem. The chromophores are mostly transition metals such as Ti, V, Cr, Mn, Fe, Cu
79 which have approximately the same atomic radius as the substituted major element(s) of the
80 mineral. On the other hand, the exceptional optical quality of gemstones make them an object
81 of choice for the study of solid and fluid inclusions (FI) trapped during their growth, and these
82 are sometimes excellent geological and/or geographical fingerprints (Giuliani et al. 2014a).

83 This paper is focused on metamorphic gems and ornamental gemstones such as
84 Colombian and Afghan emeralds, ruby-bearing marbles in central and south-east Asia, garnet
85 vanadium-rich grossular i.e. tsavorite and vanadium-rich zoisite called tanzanite from
86 Tanzania, Kenya and Madagascar, and lapis-lazuli in marble and/or calc-silicate rocks from
87 Afghanistan (Fig. 1). Previous studies highlighted special common features: (i) the presence
88 of halite, sulphates and minerals rich in Cl, Na, Mg, B and F; and (ii) either the trapping of
89 high-salinity aqueous (\pm carbonic) FI or CO₂-H₂S-S₈-rich FI (Roedder 1963; Giuliani et al.
90 1993a; Giuliani et al. 2003; Garnier et al. 2008; Feneyrol et al. 2013; Giuliani et al. 2015a).
91 Three questions arise concerning these metamorphic gems primarily due to change in the
92 conditions of heat and pressure, and fluid-rock interactions by diffusion or percolation
93 (metasomatism): (1) the origin and the role of these fluids; (2) the nature and the importance
94 of the protolith; and (3) the characteristics of the paleogeography of the depositional
95 sedimentary environment. During this review, we will show the efficiency of different
96 analytical techniques which allow the acquisition of relevant data for answering these
97 questions.

98

99 **The geological setting of metamorphic gems**

100

101 Recent petrographical and geochemical data obtained on the formation of metamorphic
102 deposits such as Colombian and Afghan emeralds, Asian ruby-bearing marbles, tsavorite and
103 tanzanite in East Africa (Groat 2014), and lapis-lazuli of Sar-e-Sang in Afghanistan (Faryad
104 2002), allowed the characterization of the protoliths of these gem-bearing metamorphic rocks.
105 These are calcareous benches alternating with black shales (BS), initially rich in organic
106 matter (OM), with intercalation of levels of evaporitic rocks. The latter are not recognizable
107 after metamorphism as such, but mineralogy and paleofluids contained in primary fluid
108 inclusions witness their past presence (Giuliani et al. 2003).

109

110 **Colombian emerald deposits**

111 Located in the Eastern Cordillera basin, the Colombian emerald deposits define two belts: the
112 eastern belt encompassing the mining districts of Gachalá, Chivor and Macanal, and the
113 western belt including the mining districts of Yacopi, Muzo, Coscuez, La Pita and Peñas
114 Blancas (Fig. 2A). Emerald mineralisation is hosted in the Lower Cretaceous sedimentary
115 series characterized by a succession of sandstone, limestone, black shale (BS), and evaporites
116 (Fig. 3). Detailed structural mapping and geometric analysis provided evidence that emerald
117 mineralisation is associated to structural events drastically different between the western and
118 eastern belts (Branquet et al. 1999a). The Muzo and Coscuez deposits are linked to tear faults
119 and associated thrusts during a compressive tectonic event whereas the eastern emerald
120 deposits, such as that of Chivor, present extensional structures extending from a brecciated
121 evaporitic level which acted as a local, gravity-driven detachment. These tectonic structures
122 are both synchronous with the circulation of hydrothermal fluids and emerald formation. The
123 fluid-rock interaction processes led to Na and Ca metasomatism of the enclosing carbonated
124 carbon-rich BS. Leaching of major (K, Al, Si, Ti, Mg, P), trace (Be, Cr, V, Rb, Sc, U, C) and
125 REE elements from the BS is accompanied by their partial redistribution to minerals in the in-
126 filling vein system, especially Cr and V which are incorporated in emerald (Giuliani et al.
127 1993b). Emerald formed at a temperature (T) ~ 300-330°C and a pressure (P) ~ 0.5-1.2 kbar
128 which correspond to a depth about 4 to 5 km (Cheilletz et al. 1994; Ottaway et al. 1994).

129 The eastern emerald belt: the Chivor mines

130 The mines are scattered along a regional white-brecciated evaporitic unit which contains
131 emerald veins (Fig. 2B). The brecciated rock unit in the Chivor area, which is in excess of 10
132 km long and 10 m thick (Figs. 4A, B), is stratiform, i.e. parallel to the sedimentary strata, and
133 dominantly composed of a breccia (Fig. 4C) made up of fragments from the hanging wall

134 (carbonated carbon-rich BS, limestone and whitish albitite, i.e. an albitised BS) cemented by
135 carbonates and pyrite (Fig. 4D). Its formation is related to the dissolution of an evaporitic
136 horizon (Branquet et al. 2015). All the mineralized structures extend vertically from the
137 brecciated level. In the Chivor mines, emerald is located in cm- to dm-thick carbonate-pyrite-
138 bearing (Fig. 1A) listric faults, meter-wide extensional fractures injected with hydrothermal
139 breccia, and extensional sets of fractures in the albitite (Fig. 4E) and calcareous carbon-rich
140 BS of the Macanal Formation. The brecciated level, the hydrothermal fluid circulation and
141 emerald formation occurred at 65 ± 3 Ma (Cheilletz et al. 1997).

142 The western emerald zone: the Muzo and Coscuez mining districts

143 On the western side, the deposits are hectometer-sized at most and display numerous folds,
144 thrusts and tear faults (Fig. 5; Laumonier et al. 1996; Branquet et al. 1999a). At the Muzo
145 deposit, thrusts are characterized by the carbonated BS which overlie siliceous BS (Fig. 6).
146 All the tectonic contacts are marked by cm- to m-thick hydrothermal breccias called by the
147 local miners "cenicero", i.e. ashtray (generally, well delimited white coloured zone which has
148 the aspect of ash during the dry season). These white- or red-coloured breccias outline the
149 thrust planes, which are associated with intense hydraulic fracturing (Branquet et al. 1999b).
150 Multistage brecciation corresponds to successive fault-fluid flow pulses, and dilatant sites
151 resulting from shear-fracturing synchronous to the thrust fault propagation. Each pulse is
152 associated with: (i) emerald-bearing banded carbonate vein-like structures present throughout
153 the breccia; (ii) emerald-bearing thrust-associated carbonate veins occurring in the wall rocks
154 and composed of calcareous BS called "cama" by the local miners (emerald zone forming a
155 layer which is parallel to the thrust fault); and (iii) emerald-bearing carbonate veins initiating
156 in the breccia zone and crosscutting the wall-rocks. All of these tectonic structures are
157 associated with fluid circulation in the calcareous carbon-rich BS which induced intense
158 albitisation, carbonatisation and pyritisation. The siliceous BS called "cambiado"(zones which
159 have changed by comparison with the cama) by the local miners have no mineralisation.

160 At the Coscuez deposit, the folds and thrusts were guided by the Coscuez tear fault which
161 acted as a vertical conduit for the mineralizing fluids developed in the carbonated carbon-rich
162 BS. Hydraulic breccias (Fig. 7), formed by the opening of dilatant sites related to fluid over-
163 pressures and hydrothermal replacement, are similar to those described for the Muzo deposit.
164 The genesis of the deposit is the consequence of a compressive phase characterized by folding
165 and thrusting along tear faults formed at the Eocene-Oligocene boundary (Cheilletz et al.
166 1994) and associated with fluid overpressure. These complex structures are probably linked to

167 a basal regional décollement or detachment fault thought to be at the level of the evaporites
168 (Branquet et al. 1999a, b).

169 At the regional scale, the presence of sedimentary levels with gypsum, residues of dissolution
170 of salts (called "rute" by Colombian miners) in the Lower Cretaceous series of the Eastern
171 Cordillera and saliferous diapirs, confirm that the continental shelf series is saliferous. The
172 significant albitisation of the BS and precipitation of albite in the hydrothermal veins
173 (Branquet et al. 1999a) testifies to important brine circulations. Furthermore, at the Chivor
174 mines, the presence in the upper albitites (see Fig. 4A) of coalescent replacement of anhydrite
175 nodules into carbonates, tepee and enterolithic structures argue for the evaporitic origin of the
176 protolith (Branquet et al. 2015).

177

178 **Emerald deposits from Afghanistan**

179 The main commercial emerald deposits are centred on the Panjshir Valley, 230 km NW of
180 Kohistan (Bowersox et al. 1991; Fig. 8). The valley coincides with the Herat-Panjshir strike-
181 slip fault which was active in the Oligo-Miocene (Tapponnier et al. 1981). The emerald
182 deposits, located on the southeastern part of the Panjshir fault zone, are dated, by Ar-Ar
183 technique on micas, at 23 ± 1 Ma (Sabot et al. 2000). The Kendjt, Khalat and Gujari deposits
184 are located along the shear zone cutting Palaeozoic metasedimentary rocks formed by
185 intercalations of schist, dolomitic marble and quartzite, in the upper greenschist facies (Kazmi
186 and Snee 1989; Vapnik and Moroz 2001). Emerald is confined to quartz-ankerite-dolomite-
187 pyrite veinlets and veins linked to shear zones (Fig. 1C). The metasomatic alteration due to
188 the fluid circulation resulted in the phlogopitisation, albitisation and silicification of the wall-
189 rocks. Albitites resembling those of Colombia are described by Sabot et al. (2000). The
190 metasomatic minerals include dravite tourmaline, pyrite, albite and phlogopite. The origin of
191 chromium, vanadium and beryllium is unknown because there are no reported whole-rock
192 analysis of the emerald-hosting metamorphic formations.

193

194 **Ruby and lapis-lazuli from central and south-east Asia**

195 Ruby in marble deposits

196 One of the main worldwide sources for excellent-quality ruby with intense colour and high
197 transparency (Fig. 1D) is associated with marble deposits from central and south-east Asia
198 (Hughes 1997). The deposits occur in Afghanistan, Pakistan, Azad-Kashmir, Tajikistan,
199 Nepal, Myanmar, northern Vietnam and southern China (Garnier et al. 2008; Fig. 8). These

200 deposits are found in metamorphosed platform carbonates associated generally with marbles
201 intercalated with garnet-biotite-sillimanite- or biotite-kyanite-bearing gneisses which are
202 sometimes intruded by granitoids (Pêcher et al. 2002). The marble units consist of
203 discontinuous horizons up to 300 m in thickness, oriented parallel to the main regional
204 foliations, thrusts or shear zones related to the Cenozoic Himalayan orogenesis between 45
205 and 5 Ma (Garnier et al. 2006). The ruby mineralisation is restricted to peculiar impure
206 marble horizons. The protolith of the ruby-bearing metamorphic rocks comprises carbonates
207 enriched in detrital clays and organic matter (OM), and intercalated evaporitic layers (Fig. 3).
208 Ruby crystals occur: (i) disseminated within marbles and associated with phlogopite,
209 muscovite, scapolite, margarite, spinel, titanite, pyrite and graphite, as in Jegdalek,
210 Afghanistan; Chumar and Ruyil, Nepal; Hunza and Nangimali, Pakistan; Mogok and Mong
211 Hsu, Myanmar; and Luc Yen, Vietnam; (ii) in veinlets or gash veins, as in some occurrences
212 in northern Vietnam, and associated with phlogopite, margarite, titanite, graphite and pyrite,
213 and sometimes related to micro-shear zones, as in Nangimali in Pakistan; (iii) in pockets
214 associated with orthoclase, phlogopite, margarite, graphite and pyrite in some occurrences of
215 northern Vietnam. Gem ruby formed during the retrograde metamorphism stage at $T \sim 620-$
216 670°C and $P \sim 2.6-3.3$ kbar (Garnier et al. 2008). The aluminium and the chromophorous
217 elements of ruby originate from the marbles (Al up to 1000 ppm, V and Cr between 5 to 30
218 ppm).

219

220 Lapis-lazuli deposits

221 The antique and famous ornamental lapis-lazuli deposits at Sar-e-Sang in the north-eastern
222 part of Afghanistan (Fig. 8) occur within the high-grade metamorphic rocks of the Goran
223 series. U-Pb, K-Ar and Rb-Sr radiometric data gave a minimum Proterozoic age at 2.13 Ga
224 for the amphibolite facies metamorphism of the Goran series (Russian literature cited in
225 Hubbard et al. 1999) while $^{40}\text{Ar}/^{39}\text{Ar}$ ages of micas associated with micaschist and phlogopite
226 from ultramagnesian rocks gave a range of ages, from 17 to 22 Ma, indicative of a Miocene
227 cooling age due to Himalayan exhumation activity (Hubbard et al. 1999). The lapis-lazuli
228 formed lenses or layers in calcite and dolomite marbles containing fine lenses or more thicker
229 anhydrite levels (Kulke 1974) and white schists (Kulke and Schreyer 1973) intercalated with
230 calc-silicate rocks, amphibolites and quartzites, and occur also at the contact between granite
231 or pegmatite with marble (Faryad 2002). The thickness of the lenses and layers is between 2
232 to 6 m while the extension is between 40 to 450 m. Generally, the central part of the layers
233 formed by calcite-diopside-lazurite (Fig. 1F) is bordered, on one side, by a diopside-rich zone

234 (40 to 90 vol. %), and on the other side by a phlogopite-diopside-calc-silicate rock zone (with
235 also scapolite, tremolite, zoisite, epidote). P-T conditions of metamorphism are $T \sim 750^{\circ}\text{C}$
236 and $P \sim 13\text{-}14$ kbar (Faryad 2002).

237

238 **Garnet tsavorite and zoisite tanzanite in East Africa**

239 All tsavorite deposits are hosted in the Neoproterozoic Metamorphic Mozambique Belt
240 (NMMB) stretching from the Arabian-Nubian shield to East Antarctica, through East Africa,
241 Madagascar and Pakistan (Feneyrol et al. 2013). The economic deposits are found in Kenya,
242 Tanzania and Madagascar (Fig. 9). They formed during Neoproterozoic Himalayan-type
243 continental collision between eastern and western Gondwana blocks, between 650 and 550
244 Ma, following the complex closure of the Mozambique Ocean. Tsavorite is hosted by a
245 metasedimentary sequence (Fig. 3) formed by a succession of quartzite, kyanite \pm sillimanite-
246 biotite \pm almandine graphitic gneiss, graphitic gneiss with intercalations of calc-silicate rock,
247 meta-evaporite and marble (Olivier 2006; Feneyrol et al. 2010). The calc-silicate rocks in the
248 graphitic gneisses display enterolithic structures (Figs. 10B, C) and \pm anhydrite-diopside and
249 tsavorite nodules (Figs. 10A, D; Feneyrol et al. 2013).

250 Tsavorite is mined within primary deposits either as nodules (Type I) or in quartz veins (Type
251 II), and placers (Type III):

252 (i) Type I: the nodules (Fig. 1E) and meta-evaporite levels are stratiform and occur among
253 calc-silicates and graphitic gneisses such as in the Kenyan tsavorite belt (Fig. 9C; Fig. 10A).
254 The tsavorite-bearing nodules are scattered in the Ca-rich rocks and formed through
255 metamorphic reactions between calcareous beds or concretionary lenses and sulphate-rich
256 levels intercalated within carbon-rich shale (Fig. 10A). The nodules formed during prograde
257 metamorphism and tsavorite formed upon anhydrite or barite at $T \sim 580\text{-}690^{\circ}\text{C}$ and $P \sim 5\text{-}7$
258 kbar (Feneyrol et al. 2013).

259 In the deposits from Kenya, Tanzania and Madagascar, V and Cr contents of graphitic
260 gneisses are respectively up to 3600 ppm and 900 ppm (Fig. 3). In Tanzania, for the Merelani
261 deposit (Fig. 9C), the source of V for tsavorite is apparently graphite hosted by the graphitic
262 gneiss, which has a V content up to 2600 ppm indicating that original OM was V-rich (Olivier
263 2006). In the Lemshuku deposit (Fig. 9C), the graphite associated with the gneiss and calc-
264 silicate rocks has no V and Cr but the V and Cr contents of the graphite-bearing gneisses are
265 respectively, between 200 and 2000 ppm, and 60 and 300 ppm (Feneyrol 2012). The V and Cr
266 precursors have been consumed during the prograde metamorphism to form V and Cr-bearing
267 kyanite, graphite, muscovite, rutile, diopside, titanite or karelianite.

268 (ii) Type II: deformation played an important role in the mineralizing processes for the quartz
269 vein deposits found in Tanzania (Merelani and Ruangwa deposits; Figs. 9A, C). Vein
270 formation and hydrothermal-metasomatic fluid circulation (carbonatisation, pyritisation and
271 graphitisation) affecting the graphitic gneisses and calc-silicates were coeval with regional
272 metamorphism (Feneyrol et al. 2013). Tsavorite in veins and pockets (Fig. 1G) formed during
273 the retrograde stage at T 505-590°C and P ~ 3.6-4.9 kbar. Gem tanzanite at Merelani (Fig.
274 1H) formed later in pockets and lenses at T ~ 385-450°C and P ~ 2.2 and 3.6 kbar (Feneyrol
275 2012). It is associated with low grade metamorphic assemblages with commonly prehnite, (\pm
276 quartz) and calcium zeolites (chabazite, heulandite, mesolite, laumontite), axinite and blue
277 apatite (Wilson et al. 2009).

278

279 In conclusion, gems mentioned in this study formed during the metamorphism of sedimentary
280 carbonate platform formations containing evaporitic rocks from Neoproterozoic to Cenozoic
281 time, and at temperatures between 300 and 750°C. The question arises as to the nature of the
282 gem protolith and the geochemistry of the fluids. In the next section, we will focus on detailed
283 aspects showing the importance of evaporites in the formation of these gems and their
284 associated paragenesis.

285

286 **The mineral and geochemical fingerprints of the past presence of evaporites**

287

288 Mineralogy

289

290 In the Colombian deposits, crystals of anhydrite, halite and sometimes sylvite are trapped by
291 emerald, quartz, albite and pyrite (Giuliani et al. 1993a).

292 In the ruby deposits, variations of local chemistry of the protolith along several decimetres are
293 due to lateral facies variations which resulted in a succession of different paragenesis: (1) F-
294 aspidolite (sodic phlogopite with Na₂O between 6.2 and 6.6 wt. %, K₂O between 0.4 and 0.6
295 wt. %, and MgO between 25.8 and 26 wt. %) associated with F-phlogopite and F-paragonite
296 in the different mineralized zones of ruby, as evidenced in the Nangimali deposit in Pakistan
297 (Garnier et al. 2004); (2) anhydrite either associated with F-tremolite, - edenite, - pargasite,
298 and calcite in samples from the Hunza Valley, Pakistan, and Luc Yen, Vietnam, or included
299 in ruby with relics of spinel (Fig. 11A); (3) anhydrite and salt crystals (CaCl₂, NaCl and KCl)
300 as solid inclusions (Figs. 11C to E) in most of the rubies observed by SEM method, as in

301 Nangimali and Luc Yen deposits (Garnier et al. 2008), and (4) F-bearing minerals such as
302 dravite-uvite tourmaline and apatite indicating a low activity of water in the fluid.

303 In the tsavorite and tanzanite deposits, the presence of different metamorphic mineral
304 associations results from lateral facies variations of the initial protolith. Tsavorite from the
305 deposit of Namalulu in Tanzania, is associated with F-Na-Cl-SO₄-Li-rich minerals that
306 indicate the presence of rich precursor evaporite-bearing sediments in the protolith (Feneyrol
307 et al. 2012): (i) the Na-Ca-Cl-scapolites with Na₂O between 6.5 and 7.9 wt. % and Cl between
308 2.3 and 2.8 wt. % as well as F-tremolite (F up to 3.8 wt. %); (ii) anhydrite crystals associated
309 with F-tremolite and dolomite in lenses in dolomitic marble (Fig. 11F); (iii) F-rich titanite
310 with very high F-content (1 to 1.6 wt. % F) as well as phlogopite (2 to 4.8 wt. % F); (iv) the
311 nodules of tsavorite concentrate towards their periphery F-bearing minerals with high F⁻/OH⁻
312 ratio such as F-phlogopite (Fig. 10D) and F-apatite, testifying again to a low activity of water
313 in the fluid and a strong fluoride activity; and (v) tsavorite is associated with a rare mineral
314 described for the first time in the metamorphic environment (Feneyrol et al. 2012): the F-
315 tainiolite (Fig. 11G) {KLiMg₂(Si₄O₁₀)(F,OH)} which contains 8.9 to 9.4 wt. % F, 2 wt. %
316 LiO₂, and between 50 and 110 ppm of boron. Tainiolite is associated with a F-tremolite
317 containing 3.5 wt. % F and up to 730 ppm of lithium. Additionally, barite is observed in the
318 nodules of tsavorite at the Nadan 1 mine in Kenya (Fig. 11B).

319 At Sar-e-Sang lapis-lazuli deposit, scapolite and halogen-bearing minerals formed during
320 prograde metamorphism of carbonate-evaporite sequences: (i) scapolite with Na₂O between
321 3.8 and 12.4 wt. % and Cl between 0.3 and 4.2 wt. %; (ii) sodalite close to the ideal end-
322 member Na₄Al₆Si₆O₁₂Cl; (iii) h uyne and lazurite with compositions respectively,
323 Ca_{1.2}Al₆Si₆Cl_{0.2}O₂₉ and Na_{5.5}Ca_{0.9}Al_{5.8}Si₆Cl_{0.1}O₂₉; (iv) F-phlogopite (F ~ 1 to 3.4 wt. %); (v)
324 Na-amphibole (F-Cl-pargasite and edenite with Cl ~ 1.1 and 1.7 wt. % Cl); (vi) F-Cl-apatite
325 containing chlorine up to 6.8 wt% and fluorine up to 4.8 wt. % (Faryad 2002). The presence
326 of Na-Cl-scapolite implies an evaporitic source with NaCl provided by salt-rich layers
327 (Faryad 2002). Besides, the magnesian kyanite-sillimanite-cordierite-dravite talcschists
328 associated with these lazurite-bearing marbles result also from the metamorphism of
329 evaporites (Schreyer and Abraham 1976). The dravite contains around 2.6 wt. % Na₂O and
330 0.1 to 0.13 wt. % F.

331

332 In conclusion, all these gemstones contain F (excepted Colombian emeralds), Cl, Li, Na, Mg
333 and B mineralogical markers which testify to the importance played by the intercalations of

334 evaporitic levels in the sedimentary series which were subsequently metamorphosed during
335 orogenesis. For the Colombian emeralds, the circulation of chlorine and sodium brines in the
336 décollement zones of the basin, responsible for the albitisation of the BS coeval with emerald
337 formation, characterised the end of the subsidence of the basin which was associated with the
338 first tectonic-metamorphic episode affecting the eastern border of the Eastern Cordillera
339 basin. The second tectonic phase reactivated similar fluid circulation processes on the western
340 border. In both borders, the process for crystallisation of emerald took place in an open
341 hydrothermal-metamorphic system. In Afghanistan, the absence of detailed geology and
342 petrography of the deposits precludes any comprehensive genetic hypothesis, but the emerald
343 veins are related to shear zones and fluid circulation led to the albitisation of the schists.
344 For the other gems, the marbles or the gneisses contained intercalations of calc-silicate rocks
345 and meta-evaporites. The chemical reactions are strongly spatially limited to the nodules
346 and/or to the lenses of evaporites, which is evidence of a very low fluid circulation. The
347 formation of ruby, tsavorite, tanzanite and lapis-lazuli occurred in quasi-closed systems.

348

349 **Geochemistry of the paleo-fluids**

350 Paleo-fluids trapped as primary FI in the minerals during their growth allow accession to the
351 composition of the mineralising fluids. Different techniques are used for their characterisation
352 such as microthermometry, Raman and infrared spectrometries, crushing of FI for analysis of
353 the cations and anions, and analysis of noble gases (Samson et al. 2003). The combination of
354 these data with those obtained on the stable isotope ratios of elements such as oxygen,
355 hydrogen, sulphur and boron on minerals coeval with the gems, permits the characterization
356 of the origin and source of the different chemical elements.

357 Colombian emerald

358 Fluids trapped by emerald are commonly three-phase FI (Fig. 12A) characterized by the
359 presence of a daughter mineral, i.e. halite (NaCl). At room temperature, the cavities contain
360 75 vol. % of salty water, i.e. an aqueous brine (liquid H₂O), 10 vol. % of gas corresponding to
361 the vapour bubble (V), and 15 vol. % of halite daughter mineral (H). However, some
362 Colombian emeralds have multiphase FI presenting a liquid carbonic phase (CO₂) forming up
363 to 3 vol. % of the total cavity volume (Figs. 3A, 12B), minute crystals of calcite (Fig. 12A),
364 very rare liquid and gaseous hydrocarbons (Kozłowski et al. 1988), and sometimes two or
365 three cubes of halite (Figs. 12A, 12B), and sylvite (KCl). These H₂O-NaCl±CO₂-(Ca-K-Mg-
366 Fe-Li-SO₄) fluids (Banks et al. 2000) are NaCl saturated (~ 40 wt% eq. NaCl) and were

367 trapped at $T \sim 300\text{-}330^\circ\text{C}$ (Roedder 1963; Giuliani et al. 1993a; Cheilletz et al. 1994; Ottaway
368 et al. 1994). The high Cl/Br ratio of the fluids (between 6,300 and 18,900) indicates that the
369 strong salinity of the brines derived from dissolution of halite of evaporitic origin (Fig. 13A;
370 Banks et al. 2000). Cation exchanges, especially calcium, with the BS host rocks are strong
371 when compared to most basinal and bittern fluids (Yardley and Bodnar 2014) and due to the
372 relatively high temperature of the parent brines of emerald. Indeed, these fluids are enriched
373 in Ca (16,000 to 32,000 ppm), base metals (Fe \sim 5,000 to 11,000 ppm; Pb \sim 125-230 ppm; Zn
374 \sim 170-360 ppm), lithium (Li \sim 400-4300 ppm) and sulphates ($\text{SO}_4 \sim$ 400-500 ppm).
375 Nevertheless there is no fluorine in these fluids (Table 1). As comparison, they have a
376 composition and Fe/Cl and Cl/Br ratio (Table 1) similar to the fluids of the geothermal system
377 of Salton Sea in California (Fig. 13B; Yardley and Cleverley 2013). The K/Na ratios confirm
378 the Na-rich character of the fluids and the strong disequilibrium between K-feldspar and
379 albite, as illustrated by the huge albitisation of the BS (Fig. 14).

380 The isotopic composition of the oxygen ($\delta^{18}\text{O}$) of H_2O in equilibrium with Colombian
381 emerald, calculated at 300°C , are higher ($15.5 < \delta^{18}\text{O} < 17.1$ ‰ for the eastern belt, and 17.5
382 $< \delta^{18}\text{O} < 23.6$ ‰ for the western belt; Giuliani et al. 2000) than those of classical basinal
383 waters which have lower temperatures of formation. Besides, the range of values of isotopic
384 composition of sulphur ($\delta^{34}\text{S}$) of pyrite associated with emerald (Fig. 1A) corresponds to the
385 isotopic range of values for sulphates (marine anhydrite) of the Lower Cretaceous of
386 Colombia (Giuliani et al. 1995).

387 Afghan emerald

388 Primary multiphase halite-sylvite-bearing FI (Fig. 12C) are common for the Panjshir emeralds
389 (Kazmi and Snee 1989; Giuliani et al. 1997). The fluids associated with emerald precipitation
390 have total dissolved salts (TDS) between 300 and 370 g/l and the trapping temperature of the
391 fluid is about 400°C (Vapnik and Moroz 2001).

392 Crush-leach analyses of the electrolyte chemistry of fluid inclusions are presented in Table
393 1. The fluids are Cl-Na-rich and they contain sulphates ($140 < \text{SO}_4 < 4,300$ ppm) and lithium
394 ($170 < \text{Li} < 260$ ppm) but very low to zero fluorine contents (Table 1). The K/Na ratio of the
395 fluid inclusions confirms the disequilibrium, at $\sim 400^\circ\text{C}$, between K-feldspar and albite which
396 drives the Na-metasomatism of the metamorphic schists and the deposition of albite in the
397 veins (Fig. 14). Crushing demonstrates that fluids are dominated by NaCl with Cl/Br ratios
398 much greater than that of seawater (Fig. 13A), indicating that the salinity was derived by
399 dissolution of halite. Thus the high Cl/Br ratios are consistent with halite dissolution for the

400 origin of salinity. The diagram I/Cl versus Br/Cl (Fig. 13B) shows also that the fluid
401 inclusions have low I contents that are also typical of brines derived from evaporite
402 dissolution. They compare with Hansonburg and contemporary fluids from the Salton Sea
403 geothermal brines (Fig. 13B), both of which have dissolved evaporites (Williams and
404 McKibben 1989; Bolkhe and Irwin 1992).

405 Ruby in marble

406 Microthermometry studies combined with Raman spectroscopy of primary FI trapped by ruby
407 indicate the contemporary trapping of two types of carbonic FI (Giuliani et al. 2015a): mono-
408 to two-phase FI (Fig. 3) in the system $\text{CO}_2\text{-H}_2\text{S-(}\pm\text{ COS } \pm\text{ S}_8) \pm (\text{H}_2\text{O, } < 10 \text{ mol. \%})$ and
409 polycrystalline FI (Fig. 12D) in the system $(\text{Na-K-Ca-CO}_3\text{-SO}_4\text{-NO}_3\text{-Cl-F}) \pm (\text{CO}_2\text{-}$
410 $\text{H}_2\text{S}) \pm (\text{H}_2\text{O})$. The different solids in the polycrystalline FI are mixtures of carbonates with
411 Ca-Na-Al cations, such as shortite and dawsonite, sulphates - mainly anhydrite and barite,
412 phosphates (F-apatite), nitrates, fluorides (fluorite), and chlorides (halite, Ca and K chlorides).
413 These solids are daughter minerals (Fig. 12D) of ionic liquids formed during the
414 metamorphism of evaporites and limestones (Giuliani et al. 2015a). As comparison, the
415 polycrystalline inclusions represent for ruby the product of crystallization of molten salts,
416 while for granites they are interpreted as the products of crystallization of silicate melts. In
417 ruby, these polycrystalline FI are rare because if the salts are not immediately trapped by the
418 crystals they are removed due to their strong solubility in water-rich fluids.

419 Crushing and leaching of rubies (Giuliani et al. 2015a) have shown that chloride is the
420 dominant anion (25 to 53 mol. %) followed by sulphate (2 to 36 mol. %), nitrate (2 to 17
421 mol. %) and fluoride (0 to 25 mol. %). Sodium is the dominant cation (16 to 42 mol. %). The
422 Li contents are very low (0.3 to 9 mol. %). The presence of nitrate, detected by both Raman
423 spectroscopy and crush-leach techniques, is a strong argument for a continental input to the
424 original sediment as, generally, nitrate salts precipitate in closed basin playas or salars
425 (Ericksen 1983). In addition, the isotopic variation of sulphur of the anhydrites included in
426 ruby and marble defines two sets of $\delta^{34}\text{S}$ values: the first, between 27 and 23 ‰, for a marine
427 anhydrite; the second, between 4.8 and 1.6‰, for a continental source (Garnier et al. 2008).

428 Tavorite and Tanzanite

429 The primary FI trapped by both minerals belong to the $\text{H}_2\text{S-S}_8 (\pm \text{N}_2 \pm \text{CH}_4)$ system (Fig.
430 12E). Crush-leach analyses of tavorite have shown that sulphate is the dominant anion (up to
431 50 mol. %) while lithium is absent and fluoride is very low (0 to 4 mol. %; unpublished data).
432 SIMS in situ analyses of dravite tourmaline associated with nodules of tavorite from Kenya,

433 Tanzania and Madagascar (Fig. 15) showed similar isotopic compositions of $\delta^{11}\text{B} = -19.8 \pm$
 434 1.2‰ (n= 7). The range of boron isotopic composition ($-20 < \delta^{11}\text{B} < -18.5 \%$; Giuliani et al.
 435 2015b) clearly indicates continental evaporitic materials and confirms the genetic model
 436 proposed for the formation of tsavorite in the metasedimentary series of the NMMB (Feneyrol
 437 et al. 2013). The sediments were derived from an ancient platform in a widespread and
 438 shallow evaporite-bearing epi-continental platform with alternation of marine and non-marine
 439 seaways on the border of the Mozambican Ocean.

440 Lapis-lazuli

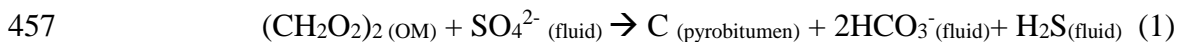
441 Up to now the observations on the paragenesis associated with lapis-lazuli have not revealed
 442 the presence of cavities of FI or polycrystalline inclusions. Different minerals formed during
 443 the prograde and retrograde metamorphic stages. At peak P-T metamorphism, the presence of
 444 scapolite with diopside, grossular, calcite and quartz implies high CO_2 and NaCl
 445 concentrations in the fluid phases ($X_{\text{CO}_2} = 0.03-0.15$ and X_{NaCl} between 0.04 and 0.99; Faryad
 446 2002). During the retrograde stage, lazurite precipitated with sodalite, haüyne, F^- or Cl^- -rich
 447 apatite, amphibole, scapolite, clinohumite and sometimes biotite.

448

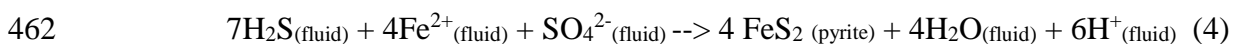
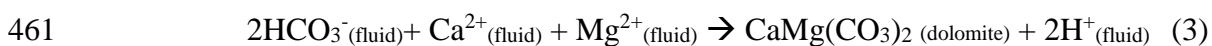
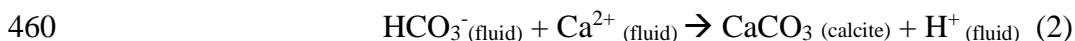
449 Discussion on the role of evaporites in the formation of metamorphic gems

450

451 Parental brines of Colombian emeralds are responsible for the albitisation of the BS. They are
 452 at the origin of the mobilisation, under the form of chlorine and fluoride complexes, of
 453 aluminium, beryllium (Wood 1992), chromium (Vasin et al. 2004), vanadium (Povolov et al.
 454 2007) and iron present in the BS. Sulphates are very sensitive to the conditions of thermal
 455 reduction, and in the presence of OM, the sulphate is reduced to sulphide (Machel et al.
 456 1995), and OM is oxidized to CO_2 and then transformed into HCO_3^- :

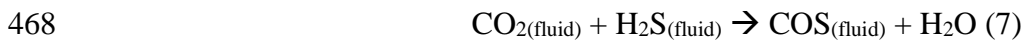
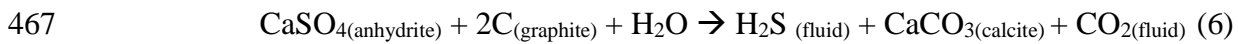
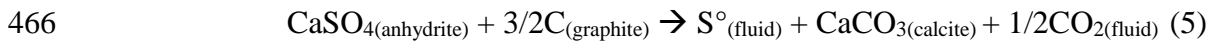


458 Products of this thermal reduction of sulphate in the presence of OM are involved in the
 459 formation of carbonates and sulphides (Giuliani et al. 2000):



463

464 In the case of ruby hosted in marble, these redox reactions are also proposed to explain the
 465 association of pyrite and calcite with ruby (Giuliani et al. 2003):



469 These reactions explain : (i) the involvement of anhydrite in these reactions, i.e. the presence
470 of anhydrite crystals included in ruby and in marble shows that the reaction progress was not
471 achieved to completion; (ii) the formation of CO₂ by oxidation of organic matter under
472 graphitisation and/or graphite; (iii) the formations of native sulphur (reaction 5); (iv) the
473 consumption of H₂O (reaction 6); and (v) the formation of COS gas in the primary fluid
474 (reaction 7), a rare component in geological fluids, that implies H₂O-poor fluids.

475 The presence of SO₄²⁻, NO₃⁻, CO₃²⁻, BO₃⁻ and F⁻ decreased consequently the temperature of
476 melting of halite and other salts, and allowed the formation of chlorine and fluorine-bearing
477 ionic liquids. The fluorine of continental origin probably played an important role in the
478 extraction of the aluminium present in the impurities (clays) of the impure limestone. For
479 comparison, the fluorine and aluminate-rich flux method is used by industry for the
480 production of Al by electrolysis due to the formation of AlF⁴⁻ complexes (e.g. Lacassagne et
481 al. 2002). So, the existence of an ionic liquid trapped in the form of polycrystalline solids by
482 the ruby explains the colour and clarity of the ruby by: (i) the mobilization of Al, Cr and V
483 contained in the metamorphosed limestone (Al ~ 1 000 ppm, Cr and V ~5 to 30 ppm for the
484 Nangimali deposit in Pakistan); and (ii) their incorporation in an isotropic and fluid
485 environment allowing crystalline growth with a minimum of defects (Giuliani et al. 2015a).

486 For tsavorite and tanzanite, the presence of anhydrite or barite in the tsavorite-bearing nodules
487 as well as H₂S-S₈-bearing FI in tsavorite points out the importance of halite and sulphates in
488 the gem formation. The notable quantity of F⁻ and Cl⁻ in phlogopite, titanite and scapolite
489 associated with tsavorite, suggests that these elements have played a leading role in the
490 mobilization of Al, and of V and Cr-bearing phengites and organic matter included in the
491 anhydrite during the prograde metamorphism (Figs. 16B, 16C; Olivier 2006; Feneyrol et al.
492 2013).

493 For lapis-lazuli, the reduction of sulphates (Faryad 2002), at T ~ 750°C and P ~ 13-14 kbar, in
494 the upper amphibolite to granulite facies, played a key role in its formation since blue colour
495 results from the absorption of visible light by the radical S³⁻ present in its structure (Reinen
496 and Lindner 1999). The radical S³⁻ was highlighted recently experimentally in aqueous fluids
497 (Pokrovski and Dubrovinsky 2011; Pokrovski and Dubessy 2014) and also those resulting

498 from the thermal reduction of sulphate (Truche et al. 2014). The evaporitic protolith
499 associated with lapis-lazuli formed an almost anhydrous chemical system which suggests that
500 the S³⁻ radical could be stable also in ionic liquids originating from the melting and thermal
501 reduction of evaporites at high temperature.

502

503 The set of geological and geochemical data obtained on these different deposits confirms the
504 presence in the protoliths of evaporites, of either continental or marine origin, which are
505 considered as a key feature in the metamorphic model for these gems (Fig. 16). They would
506 have formed during the metamorphism, from the greenschist to granulite facies, of carbonates
507 interbedded with OM-bearing mudstones, and containing intercalations of sulphates-
508 chlorides-nitrates-borates of impure evaporitic rocks. The lithological control of the
509 mineralisation is essential. These particular sedimentary lithologies and the nature of the
510 metamorphic piles permit the delineation of the paleogeography of the depositional
511 sedimentary environment. The sedimentary landscape converged to an epeiric carbonate
512 platform succession with a combination of saltern and evaporite mudflats of gypsum and
513 anhydrite such as described by Warren (2006).

514 The separation of the pericontinental and epicontinental seaways implies the presence of a
515 sedimentary or a tectonic barrier, and at times the shallow epeiric seaway was converted to
516 saltern mudflat (sabkha) with continental inputs. The presence of carbonate or siliciclastic
517 and/or evaporitic matrix in the rocks is indicative of sediment deposited in a continental zone
518 which was temporarily flooded by the tides, such as proposed for ruby hosted in
519 metasediments (Garnier et al. 2008). The marine coastal sabkha environment is characterized
520 by the formation of gypsum and anhydrite crystals, and nodules typically with enterolithic and
521 'chicken-wire' textures confirming their formation in supratidal zones such as described for
522 the Colombian BS series and the Tanzanian and Kenyan metamorphosed BS formations. The
523 high concentration of graphite in some metamorphic levels in the Kenyan Neoproterozoic
524 tsavorite belt may represent original microbial mats (Feneyrol et al. 2013).

525

526 **Perspectives**

527

528 In spite of their differences in chemical composition, crystallisation system, physical
529 conditions of metamorphism (P-T), scale of fluid circulation and ages, these metamorphic
530 gemstones have in common a geochemical history connected to the nature of their mother
531 protoliths.

532 Their mineralogical, chemical and isotopic characteristics are witnesses of fluid-rock
533 interactions in open or closed systems. The understanding of their geological formation is one
534 of the keys for the identification of their origin. The mineral and fluid inclusions trapped by
535 gems during the metamorphism of rocks in carbonate platform successions are precious
536 markers for understanding the genesis of the gems. The nature and chemical composition of
537 the inclusions highlight the major contribution of evaporites by dissolution (for Colombian
538 and Afghan emeralds) or melting (for other gems), depending of their temperature of
539 formation. Solubility experiments of these gems in chloride-fluoride ionic liquids should be
540 done together with speciation studies of the different chemical components involved in these
541 minerals in order to generate thermodynamic models of such metamorphic ionic liquids.
542 Other worldwide deposits such as lapis-lazuli in Myanmar, Russia and Baffin Island in
543 Canada, emeralds from Davdar and Musakashi, respectively in China and Zambia,
544 Precambrian sodalite from Bahia state in Brazil, lazulite in the Neoproterozoic Itremo
545 quartzite from central Madagascar, now suggest investigation of the possible presence of
546 evaporites in the formation of these high-value and ornamental gems. Guidelines for
547 prospecting new gem deposits of metamorphosed carbonate platform-related areas worldwide
548 include: (i) the lithological control of the mineralisation from an ancient platform evaporite
549 environment with alternation of marine and non-marine seaways, i.e. a marine coastal sabkha-
550 like environment; (ii) the presence of index minerals such as anhydrite, scapolite, aspidolite,
551 and chloride-fluoride-sulphate \pm carbonate-rich fluid inclusions which can decipher the major
552 contribution of evaporites by their dissolution or fusion, depending of their temperature of
553 formation.

554

555 **Acknowledgements**

556 The authors would like to thank Dr. Bernd Lehmann, Editor of *Mineralium Deposita*, who
557 invited us to write this paper on the role of evaporites in the formation of metamorphic gems,
558 published in a short version as "Le fluide, l'Arlésienne du métamorphisme" in the *Journal*
559 *Géochronique*, N°136, décembre 2015 entitled "Regards croisés sur le métamorphisme".

560

561 **References**

- 562 Banks D, Giuliani G, Yardley BWD, Cheilletz A (2000) Emerald mineralisation in Colombia:
563 fluid chemistry and the role of brine mixing. *Miner Deposita* 35: 699-713
564 Barth S (1993) Boron isotope variations in nature - a synthesis. *Geol Rundschau* 83: 640-651

565 Bohlke JK, Irwin JJ (1992) Laser microprobe analyses of Cl, Br, I and K in fluid inclusions -
566 implications for sources of salinity in some ancient hydrothermal fluids. *Geochim*
567 *Cosmochim Acta* 56: 203-225

568 Bowersox GW, Snee LW, Foord EF, Seal RRII (1991) Emeralds of the Panjshir Valley,
569 Afghanistan. *Gems & Gemology* 27: 26-39

570 Branquet Y, Laumonier B, Cheilletz A, Giuliani G (1999a) Emeralds in the Eastern Cordillera
571 of Colombia: Two tectonic settings for one mineralisation. *Geology* 27: 597-600

572 Branquet Y, Cheilletz A, Giuliani G, Laumonier B (1999b) Fluidized hydrothermal breccia in
573 dilatant faults during thrusting: the Colombian emerald deposits. In: McCaffrey KJW,
574 Lonergan L, Wilkinson JJ (eds) *Fractures, fluid Flow and Mineralisation*. Geological
575 Society, London, United Kingdom, Special Publications, 155, pp 183-195

576 Branquet Y, Giuliani G, Cheilletz A, Laumonier B (2015) Colombian emeralds and
577 evaporites: tectono-stratigraphic significance of a regional emerald-bearing evaporitic
578 breccia level. In: André-Mayer AS, Cathelineau M, Muecher Ph, Picard E, Sindern S (eds)
579 *From source, transport and metal deposits to mineral resources in a sustainable world*,
580 *Proceedings of the 13th biennial meeting of the Society for Geology Applied to Mineral*
581 *Deposits*, Nancy, France, pp 1291- 1294

582 Cheilletz A, Féraud G, Giuliani G, Rodriguez CT (1994) Time-pressure-temperature
583 formation of Colombian emerald: an $^{40}\text{Ar}/^{39}\text{Ar}$ laser-probe and fluid inclusion-
584 microthermometry contribution. *Econ Geol* 89: 361-380

585 Cheilletz A, Giuliani G, Branquet Y, Laumonier B, Sanchez AJM, Féraud G, Arhan T (1997)
586 Datation K-Ar et $^{40}\text{Ar}/^{39}\text{Ar}$ à 65 ± 3 Ma des gisements d'émeraude du district de Chivor-
587 Macanal: argument en faveur d'une déformation précoce dans la Cordillère Orientale de
588 Colombie. *C R Acad Sci* 324: 369-377

589 Ericksen GE (1983) The Chilean nitrate deposits. *Am Sci* 71: 366-374

590 Faryad SW (2002) Metamorphic conditions and fluid compositions of scapolite-bearing rocks
591 from the lapis lazuli deposit of Sare Sang, Afghanistan. *J Petrol* 43: 725-747

592 Feneyrol J (2012) *Pétrologie, géochimie et genèse des gisements de tsavorite associés aux*
593 *gneiss et roches calco-silicatées graphiteux de Lemshuku et Namalulu (Tanzanie)*. Ph.D
594 Institut National Polytechnique de Lorraine, Vandœuvre-lès-Nancy, France

595 Feneyrol J, Giuliani G, Ohnenstetter D, Le Goff E, Malisa PJ, Saul M (2010)
596 Lithostratigraphic and structural controls of tsavorite deposits at Lemshuku, Merelani area,
597 Tanzania. *Contrôles lithostratigraphique et structural des gisements de tsavorite de*
598 *Lemshuku, région de Merelani, Tanzanie*. *C R Acad Sci* 342: 778-785

599 Feneyrol J, Ohnenstetter D, Giuliani G, Fallick AE, Rollion-Bard Cl, Robert JL, Malisa E
600 (2012) Evidence of evaporites in the genesis of the vanadian grossular tsavorite deposit in
601 Namalulu, Tanzania. *Can Mineral* 50: 745-769

602 Feneyrol J, Giuliani G, Ohnenstetter D, Fallick AE, Martelat JM, Monié P, Dubessy C,
603 Rollion-Bard Cl, Le Goff E, Malisa E, Rakotondrazafy AFM, Pardieu V, Kahn T, Ichang'i,
604 D, Venance E, Voarintsoa NR, Ranatsenho M, Simonet C, Omito E, Nyamai C, Saul M
605 (2013) Worldwide tsavorite deposits: new aspects and perspectives. *Ore Geol Rev* 53: 1-25

606 Fritz H, Abdelsalam M, Ali KA, Bingen B, Collins AS, Fowler AR, Ghebread W,
607 Hauzenberger CA, Johnson PR, Kusky TM, Macey P, Muhongo S, Stern RJ, Viola G
608 (2013) Orogen styles in the East Africa region: a review of the Neoproterozoic to
609 Cambrian tectonic evolution. *J Afr Earth Sci* 86: 65-106

610 Garnier V, Ohnenstetter D, Giuliani G (2004) L'aspidolite fluorée: rôle des évaporites dans la
611 genèse des marbres de Nangimali (Azad-Kashmir, Pakistan). *C R Acad Sci* 336: 1245-
612 1253

613 Garnier V, Maluski H, Giuliani G, Ohnenstetter D, Schwarz D (2006) Ar-Ar and U-Pb ages
614 of marble-hosted ruby deposits from central and southeast Asia. *Can J Earth Sci* 43: 509-
615 532

616 Garnier V, Giuliani G, Ohnenstetter D, Fallick AE, Dubessy J, Banks D, Hoàng Quang V,
617 Lhomme Th, Maluski H, Pêcher A, Bakhsh KA, Pham Van L, Phan Trong T, Schwarz D
618 (2008) Marble-hosted ruby deposits from central and Southeast Asia: towards a new
619 genetic model. *Ore Geol Rev* 34: 169-191

620 Giuliani G, Cheillett A, Dubessy J, Rodriguez CT (1993a) Emerald deposits from Colombia:
621 chemical composition of fluid inclusions and origin. In: Nägele u. Obermiller (eds)
622 Proceedings of the 8th biennial IAGOD symposium, Ottawa, Canada. pp 159-168

623 Giuliani G, Cheillett A, Sheppard SMF, Arboleda C (1993b) Geochemistry and origin of the
624 emerald deposits of Colombia. In: Hach-Ali F, Torres L and Gervilla F (eds) Current
625 research in geology applied to ore deposits, Proceedings of the 2nd biennial meeting of the
626 Society for Geology Applied to Mineral Deposits, Granada, Spain, pp 105-108

627 Giuliani G, Cheillett A, Arboleda C, Rueda F, Carillo V, Baker J. (1995) An evaporitic origin
628 of the parent brines of Colombian emeralds: fluid inclusion and sulfur isotopic evidence. *Eur*
629 *J Mineral* 7: 151-165

630 Giuliani G, France-Lanord C, Zimmermann JL, Cheillett, A, Arboleda C, Charoy B, Coget P,
631 Fontan F, Giard D (1997) Composition of fluids, δD of channel H_2O and $\delta^{18}O$ of lattice

632 oxygen in beryls: genetic implications for Brazilian, Colombian and Afghanistani emerald
633 deposits. Intern Geol Rev 39: 400-424

634 Giuliani G, France-Lanord Ch, Cheilletz A, Coget P, Branquet Y, Laumonier B (2000)
635 Sulfate reduction by organic matter in Colombian emerald deposits: chemical and stable
636 isotope (C, O, H) evidence. Econ Geol 95: 1129-1153

637 Giuliani G, Dubessy J, Banks D, Hoang Quang V, Lhomme T, Pironon J, Garnier V, Phan
638 Trong T, Pham Van L, Ohnenstetter D, Schwarz D (2003) CO₂-H₂S-COS-S₈-AlO(OH)-
639 bearing fluid inclusions in ruby from marble-hosted deposits in Luc Yen area, North
640 Vietnam. Chem Geol 194: 167-185

641 Giuliani G, Groat L, Ohnenstetter D, Fallick AE, Fenevrol J (2014a) The geology of gems
642 and their geographic origin. In: Raeside ER (ed) Geology of Gem Deposits, Mineralogical
643 Association of Canada, Short Course Series 44, Tucson, USA, pp 113-134

644 Giuliani G, Ohnenstetter D, Fallick AE, Groat L, Fagan J (2014b) The geology and genesis of
645 gem corundum deposits In: Raeside ER (ed) Geology of Gem Deposits, Mineralogical
646 Association of Canada, Short Course Series 44, Tucson, USA, pp 29-112

647 Giuliani G, Dubessy J, Banks D, Lhomme Th, Ohnenstetter D (2015a) Fluid inclusions in
648 ruby from Asian marble deposits: genetic implications. Eur J Mineral 27: 393-404

649 Giuliani G, Ohnenstetter D, Rollion Cl, Fenevrol J, Martelat JE, Omito E, Ichang'i D, Nyamai
650 Ch, Wamunyu A (2015b) The boron isotopic composition of tourmaline from tsavorite
651 deposits in the Neoproterozoic Mozambique metamorphic belt, with a special focus on the
652 mining districts in Kenya. In: André-Mayer AS, Cathelineau M, Muchez Ph, Picard E,
653 Sondern S (eds) From source, transport and metal deposits to mineral resources in a
654 sustainable world, Proceedings of the 13th biennial meeting of the Society for Geology
655 Applied to Mineral Deposits, Nancy, France, pp 1319-1322

656 Groat L.A. (2014) Geology of Gem Deposits. Mineralogical Association of Canada Short
657 Course series 44, Raeside R. (ed), Tucson Arizona, USA

658 Hubbard MS, Grew ES, Hodges KV, Yates MG, Pertsev NN (1999) Neogene cooling and
659 exhumation of upper-amphibolite-facies 'whiteschists' in the southwest Pamir Mountains,
660 Tajikistan. Tectonophysics 305: 325-337

661 Hughes R.W. (1997) Ruby and Sapphire, RW Hughes publishing, Boulder, USA

662 Kazmi AH, Snee LW (1989) Emeralds of Pakistan, Van Nostrand Reinhold, New York, USA

663 Kozlowski A, Metz P, Jaramillo HAE (1988) Emeralds from Sodomondoco, Colombia:
664 chemical composition, fluid inclusion and origin. Neues Jahrbuch Miner Abh 59: 23-49

665 Kulke HG (1974) Die lapis-lazuli Sar-e-Sang (Badakhshan): geologie, entstehung,
666 kulturgeschichte und bergbau. Afghanistan Journal: 43-56

667 Kulke HG, Schreyer W (1973) Kyanite-talc schist from Sar e Sang, Afghanistan. Earth Planet
668 Sci Lett 18: 324-328

669 Lacassagne V, Bessedat C, Florian P, Bouvet S, Olliver B, Coutures JP, Massiot D (2002)
670 Structure of high temperature NaF-AlF₃-Al₂O₃ melts: a multinuclear NMR study. J Phys
671 Chem 106: 1862-1868

672 Laumonier B, Branquet Y, Cheilletz A, Giuliani G, Rueda F (1996) Les gisements
673 d'émeraude de Muzo et de Coscuez (ouest de la Cordillère Orientale de Colombie) sont des
674 duplex formés pendant une phase de tectonique en chevauchement à la limite Eocène-
675 Oligocène. C R Acad Sci 320: 1171-1178

676 Machel HG, Krouse HR, Sassen R (1995) Products and distinguishing criteria of bacterial and
677 thermochemical sulphate reduction. Appl Geochem 10: 373-389

678 Mattauer M, Matte Ph, Jolivet JL, (1999) A 3D model of the India-Asia collision at plate
679 scale: C R Acad Sci 328: 499-508

680 Olivier B (2006) The geology and petrology of the Merelani tanzanite deposit, NE Tanzania.
681 Ph.D University of Stellenbosch, South Africa

682 Ottaway TL, Wicks FJ, Bryndzia LT, Kyser TK, Spooner ETC (1994) Formation of the Muzo
683 hydrothermal emerald deposit in Colombia. Nature 369: 552-554

684 Pêcher A, Giuliani G, Garnier V, Maluski H, Kausar AB, Malik RM, Muntaz HR (2002)
685 Geology and Geochemistry of the Nangimali ruby deposit area, Nanga-Parbat Himalaya
686 (Azad Kashmir, Pakistan). J Asian Earth Sci 21: 265-282

687 Pokrovski GS, Dubrovinsky LS (2011) The S³⁻ ion is stable in geological fluids at elevated
688 temperatures and pressures. Science 331: 1052-1054

689 Pokrovski GS, Dubessy J (2014) Stability and abundance of the trisulfur radical ion S³⁻ in
690 hydrothermal fluids. Earth Planet Sci Lett 411: 298-309

691 Polovov IB, Vasin BD, Abakumov AV, Rebrin OI, Chernyshov MV, Volkovich VA, Griffiths
692 TR (2007) Thermodynamics of the formation of vanadium (II) complexes in chloride
693 melts. In: Mantz RA, Hagiwara M, Trulove HC, De Long H, Stafford GR, Fox D (eds)
694 "Molten Salts", ECS Transactions" 3, Issue 35, The Electrochemical Society, Pennington,
695 pp 589-597

696 Reinen D, Lindner GG (1999) The nature of chalcogen colour centres in ultramarine-type
697 solids. Chem Soc Rev 28: 75-84

698 Roedder E (1963) Studies of fluid inclusions II: freezing data and their interpretation. *Econ*
699 *Geol* 58: 163-211

700 Sabot B, Cheilletz A, De Donato P, Banks D, Levresse D, Barrès O (2000) Afghan emeralds
701 face Colombian cousins. *Chron Rech Min* 541: 111-114

702 Samson I, Anderson A, Marshall D (2003) Fluid inclusions: Analysis and interpretation.
703 Mineralogical Association of Canada, Short Course series 32, Raeside R. (ed), Vancouver,
704 British Columbia, Canada

705 Schreyer W, Abraham K (1976) Three-stage metamorphic history of a whiteschist from Sar e
706 Sang, Afghanistan, as part of a former evaporite deposit. *Contrib Mineral Petrol* 59: 111-
707 130

708 Tapponnier P, Mattauer M, Proust F, Cassaigneau Ch (1981) Mesozoic ophiolites, sutures,
709 and large-scale tectonic movements in Afghanistan. *Earth Planet Sci Lett* 52: 355-371

710 Tenczer V, Hauzenberger C, Fritz H, Hoinkes G, Muhongo S, Klötzli U (2013) Crustal age
711 domains and metamorphic reworking of the deep crust in Northern-Central Tanzania: a
712 U/Pb zircon and monazite age study. *Mineral Petrol* 107: 679-707

713 Truche L, Bazarkina EF, Barré G, Thomassot E, Berger G, Dubessy J, Robert P (2014) The
714 role of S³⁻ ion in thermochemical sulphate reduction: geological and geochemical
715 implications. *Earth Planet Sci Lett* 396: 190-200

716 Van Hinsberg VJ, Henry DJ, Marschall HR (2011) Tourmaline: an indicator of its host-
717 environment. *Can Mineral* 49: 1-16

718 Vapnik YE, Moroz I (2001) Fluid inclusions in Panjshir emerald (Afghanistan). In: Noronha
719 F, Dória A, Guedes A (eds), XVI European current research on fluid inclusions, (ECROFI),
720 Porto, Portugal, Faculdade de Ciências do Porto, Memoria 7, pp 451-454

721 Vasin BD, Polovov IB, Volkovich VA, Griffiths TR, Berezin AV (2004) Coordination state
722 of vanadium in chloride melts: an electronic absorption spectroscopy study. In: Mantz RA,
723 Trulove HC, De Long H, Stafford GR, Hagiwara M, Costa DA (eds) "Molten Salts XIV",
724 Proceedings of the International symposium, Electrochemical Society, 2004-24, New
725 Jersey, USA, pp 261-268

726 Warren JK (2006) *Evaporites: Sediments, Resources and Hydrocarbons*. Springer, Berlin,
727 Germany

728 Williams AE, McKibben MA (1989) A brine interface in the Salton Sea Geothermal system,
729 California: fluid, geochemical and isotopic characteristics. *Geochim Cosmochim Acta* 53:
730 1905-1920

731 Wilson WE, Saul JM, Pardieu V, Hughes RW (2009) The Merelani tanzanite mines. Mineral
732 Record 40: 347-408

733 Wood SA (1992) Theoretical prediction of speciation and solubility of beryllium in
734 hydrothermal solution to 300°C at saturated vapour pressure: application to
735 bertrandite/phenakite deposits. Ore Geol Rev 7: 249-278

736 Yardley WB, Cleverley JS (2013) The role of metamorphic fluids in the formation of ore
737 deposits. In: Jenkin GRT, Lusty PAJ, McDonald I, Smith MP, Boyce AJ, Wilkinson JJ
738 (eds), Ore Deposits in an Evolving Earth. Geol Soc London, Special Publications 393. doi:
739 10.1144/SP393.5

740 Yardley WB, Bodnar RJ (2014) Fluids in the continental crust. Geochem Persp Lett 3: 1-127

741

742

743

744 **Figure captions**

745 **Figure 1.** Metamorphic gems. A- Crystal of emerald on pyrite, Chivor mines, eastern
746 emerald belt, Colombia, 3.9x2.6 cm. Collection MultiAxes. B- Association of emerald and
747 quartz, Muzo mines, western emerald belt, Colombia. C- Emerald crystals on quartz and
748 adularia, Panjshir Valley, Afghanistan, 6.6x4.4 cm. Specimen Fine Art Mineral. D- Ruby
749 crystal associated with flakes of phlogopite in a marble matrix, Minh Tien mine, Luc Yen
750 mining district, Vietnam, 2x1 cm. E- Nodule, rough and cut of tsavorite from the Tsavolite
751 mine, Mangare mining district, Voi region, Kenya, diameter of the nodule (on the left) ~ 3.5
752 cm. F- Association lazurite, carbonate and pyrite from Sar-e-Sang mines, Afghanistan,
753 8.3x6.2 cm, Specimen Crystal Classics. G- Gem crystal of tsavorite (2 cm across) embedded
754 in a graphitic gangue with calcite (white), Merelani mines, Arusha district, Tanzania. H- Blue
755 zoisite, variety tanzanite, Merelani, Arusha district, Tanzania, 8.7x5x3 cm. Collection Marcus
756 Budil. Photos: A to C, F to H, L.-D. Bayle/le Règne Minéral. Photo D: G. Giuliani. Photo E:
757 V. Pardieu/GIA.

758 **Figure 2.** Colombian emerald mines (modified from Branquet et al. 2015). A- Simplified
759 geological map of the Colombian Eastern Cordillera with the location of the main emerald
760 deposits. Inset is location of Figure 2B. B- Geological map of the Chivor area. All emerald
761 and gypsum deposits and occurrences are hosted within the upper Guavio Formation.

762 **Figure 3.** Geological features of Cr-V-bearing metamorphic gems formed during the
763 metamorphism of rocks (black shale-carbonate-sandstone with evaporite intercalations) from

764 carbonate platform successions. Be: beryllium; Al: aluminium; Si: silica; Ca: calcium; Cr:
765 chromium; V: vanadium. Colombian emerald deposits: a: Mg-limestone; b: emerald-bearing
766 calcareous C-rich BS; c: sandstone; d: pyritic nodules in siliceous BS; e: siliceous BS. Ruby
767 in marble from central and south-east Asia: f: quartzite; g: amphibolite; h: mica-bearing
768 marble; i: pyrite-bearing marble; j: calc-schist and garnet-biotite micaschist; k: ruby-
769 anhydrite-bearing yellow Mg-marble; l: white dolomite and/or calcite marbles. Tsavorite in
770 graphitic gneiss and calc-silicates from Tanzania: m: biotite-kyanite gneiss; n: graphitic
771 gneiss; o: tsavorite-bearing nodules in graphitic gneiss and calc-silicate rocks with anhydrite-
772 gypsum veinlets or lenses; p: calc-silicate rocks; q: kyanite-graphite gneiss; r: dolomitic
773 marble with anhydrite levels (modified from Giuliani et al. 2014b).

774 **Figure 4.** A- Geological cross-section through the Chivor emerald deposits, eastern
775 emerald belt (from Branquet et al. 2015). B- South-eastern field view of the cross-section. C-
776 Chivor Klein pit. Upper contact of the main breccia level (in black) with albitites (1). The
777 transport of clasts of albitite (2) within the breccia is marked by tails. D- Oriente deposit.
778 Polygenic breccia formed by clasts of albitite (Ab) and black shales (Bs), cemented by pyrite,
779 carbonates and albite. E- Oriente deposit. Carbonate (Cb) -pyrite (Py) -emerald-bearing veins
780 crosscutting albitite (Ab) showing some remnants of black shale (Bs). The greyish tracks
781 parallels to the carbonate veins are residues of dust not cleaned by the water jet in the mine.
782 Photos B to D: Y. Branquet and Photo E: G. Giuliani.

783 **Figure 5.** Geological map of the Tequendama and Quipama mines, Muzo mining district,
784 western emerald belt. U1 through U4 represent the different tectonic units. The cross-section
785 A-B is drawn on figure 6. Modified from Laumonier et al. (1996).

786 **Figure 6.** Cross-section of the Tequendama mine located at the northern part of the Muzo
787 emerald mining district (A-B section as shown on Figure 5). The deposit is linked to tear
788 faults and associated thrusts which are marked by the overlying of the siliceous black shales
789 by the carbonated ones. The thrust planes are underlined by a hydrothermal breccia (called
790 "cenicero" by the miners) and hydraulic fracturing. The fluid circulation induced intense
791 albitisation, carbonatisation and pyritisation of the surrounding black shales (modified from
792 Branquet et al. 1999b).

793 **Figure 7.** Hydraulic fracturing breccia of black shale located in the tear fault of Coscuez
794 mine, western Colombian emerald belt. Photo: Y. Branquet.

795 **Figure 8.** Location of the Panjshir emerald and Sar-e-Sang lapis-lazuli deposits in
796 Afghanistan, and ruby-hosted marble from central and south-east Asia. The main tectonic
797 structures and blocks are reported from Mattauer et al. (1999): CF: Chaman fault, GF:
798 Gaoligong fault, SF: Sagain fault, RRF: Red River fault, HK: Hindu Kush, K: Kohistan, P:
799 Pamir.

800 **Figure 9.** (A) Tectonic map of Kenya and Tanzania (modified after Fritz et al. 2013) with
801 the localities of the main tsavorite and tanzanite deposits. (B) Tectonic map of Madagascar
802 (modified after Fritz et al. 2013) with the locality of the tsavorite deposits. (C) Geological
803 sketch map of SE Kenya and NE Tanzania (modified after Tenczer et al. 2013) with the
804 localities of the tsavorite and tanzanite. ANS: Arabian Nubian Shield; EG: Eastern Granulite;
805 WG: Western Granulite.

806 **Figure 10.** Tsavorite mineralisation from the Neoproterozoic Metamorphic Mozambique
807 Belt in southeastern Kenya and northeastern Tanzania. A- Calc-silicates band (Csb) hosting
808 diopside (Di) nodules in the graphitic gneiss (Grg) from the Davis Mine, Lualenyi mining
809 district, Mgama ridge, Kenya. B- Nodule of anhydrite (Anh) and green grossular (Grs-
810 tsavorite) presenting a 'chicken-wire' texture in a matrix composed of quartz (Qtz) and calcite
811 (Cal). The nodules are at the contact with the graphitic gneiss (Grg) which have
812 accumulations of graphite (Gr). Classic mine, eastern part of the Mgama ridge, Kenya. C-
813 Tsavorite is hosted by meta-evaporitic horizons intercalated in the graphitic gneiss (Grg). The
814 anhydrite-bearing level (Anh) is formed by nodules showing enterolithic textures and the
815 anhydrite-alunite (Sulph) level. D- Tsavorite-bearing nodule from the Komolo mine, south of
816 Arusha, northeastern Tanzania. The nodule is zoned and the mineral assemblages are, from
817 the centre to the periphery: (i) V- green grossular in the centre (Grs); (ii) the first rim (R1) is
818 formed predominantly by anhydrite (Anh) + gypsum (Gp), quartz and minor V-titanite, V-
819 zoisite and small crystals of tsavorite; (iii) the second rim (R2) contains anhydrite (Anh) +
820 gypsum, clay and minor V-free zoisite; and (iv) the external zone is the graphitic gneiss (Grg)
821 with quartz, plagioclase, K-feldspar, V-kyanite, V-muscovite, V-rutile, graphite (Gr), F-rich
822 phlogopite (Phl) and minor calcite and jarosite. Photographs A to C: G. Giuliani; D: J.
823 Feneyrol.

824 **Figure 11.** SEM images showing the presence of sulphate and salt inclusions in the gems
825 or associated minerals. A- Ruby (Crn) in equilibrium with dolomite (Dol) formed from the
826 reaction of spinel (Sp) with calcite. Spinel is a pre-ruby phase which contains high Cr (up to
827 19 wt. %) and Zn contents (10 wt. %). Spinel is associated with anhydrite (Anh). Hunza

828 Valley, Pakistan. B- The nodule of tsavorite shows remnants of barite (Brt) substituted by
829 diopside (Di), titanite (Ttn) and tsavorite (Ts), Mine of Nadan 1, Voi region, Kenya. C- Halite
830 crystal (NaCl) in ruby (Crd). Mine of Jegdalek (Afghanistan). D- Crystals of anhydrite (Anh)
831 associated with phlogopite (Phl) included in a ruby (Crd) from the Nangimali deposit, Azad
832 Kashmir, Pakistan. E- Mixtures of salts (Ca-Na-K-[Cl] and sylvite (KCl) found in ruby (Crd)
833 from the deposits of Luc Yen, Vietnam. F- Anhydrite (Anh) inclusion associated with F-
834 tremolite (F-Tr) and dolomite (Dol) in marble, Namalulu tsavorite deposit, south of Arusha,
835 northern Tanzania. G- Tainolite (Tnl) associated with calcite (Cal) in a dolomite (Dol) lens
836 from the Namalulu tsavorite deposit.

837 **Figure 12.** Parental fluids of emerald, ruby and tsavorite. A- Tabular fluid inclusion
838 trapped by a Colombian emerald (Chivor mine, eastern emerald belt). The primary cavity
839 contains a liquid (L), vapour (V), two cubes of halite (H) and a minute crystal of calcite (Cal).
840 B- Fluid inclusion in a Colombian emerald showing three cubes of halite (H), the liquid phase
841 (L), the contracted vapour phase (V), a minute black phase (S) and a thin rim of liquid carbon
842 dioxide (L₁) rim visible at the bottom part of the vapour phase. C- Multiphase primary fluid
843 inclusions trapped by an emerald from the Panjshir Valley (Afghanistan). The cavity contains
844 a vapour (V) and liquid (L) phases, a cube of halite (H), usually a primary and rounded salt of
845 sylvite (Syl) and aggregates of several unidentified anisotropic grains (S). D- Primary
846 polycrystalline fluid inclusions trapped by the Mogok ruby in marble from Myanmar. The
847 cavity contains different solids which are mixtures of carbonates, with Ca-Na-Al cations such
848 as calcite (Ca), dawsonite (Dw), shortite (Sh), and apatite (Ap), fluorite (Fl), halite (H),
849 graphite and a CO₂-H₂S-bearing fluid phase (CO₂). E- Primary multiphase H₂S-dominated FI
850 (liquid [L_{H₂S}] + vapour [V_{H₂S}]) with native sulphur (S₈), phengite (Phg) and calcite (Cal) in a
851 tsavorite from Merelani. Photos: G. Giuliani.

852 **Figure 13.** Origin of salinity in the emerald and quartz-related brines from Colombia and
853 Afghanistan. A- Analyses of the fluid inclusions from both emerald and quartz show a wide
854 range of Na/Br and Cl/Br molar ratios that are much greater than those of primary halite and
855 indicate a substantial loss of Br, typical of recrystallised halite for both emerald deposits. B-
856 Log(I/Cl) versus Log(Br/Cl) molar ratios of Afghan and Colombian fluid inclusions which are
857 depleted in both Br and I, indicative of evaporites contribution to the fluids in emerald and
858 quartz. They are compared with composition of fluids where evaporites are known to be
859 involved such as for the Salton Sea geothermal brines (Williams and McKibben 1989) and
860 Hansonburg (Bohlke and Irwin 1992).

861 **Figure 14.** Diagram log (K/Na) molar ratio versus 1/T (°K) showing the evolution of the
862 fluids associated with Colombian and Afghan emeralds relatively to crustal fluids including
863 bittern brines, brines derived by dissolution of evaporites, and magmatic fluids (modified
864 from Yardley and Bodnar 2014). Sedimentary formation brines deviate significantly from the
865 K-feldspar-albite equilibrium as well as for Afghan and Colombian brines which are
866 associated with a huge albitisation of their host-rock with the complete consumption of K-
867 feldspar from respectively, the schist and black shale.

868 **Figure 15.** Boron isotopic composition of tourmalines associated with tsavorite from
869 Kenya, Tanzania and Madagascar. The $\delta^{11}\text{B}$ (‰) of tourmalines clearly involves continental
870 evaporitic material (Feneyrol 2012). The boron isotopic ranges of other Kenyan tourmalines
871 associated with different rocks from the tsavorite-bearing metasedimentary series are reported
872 for comparison (Giuliani et al. 2015b). The different boxes representative of different
873 geological environments are from Barth (1993) and van Hinsberg et al. (2011).

874 **Figure 16.** The formation of metamorphic tsavorite-bearing nodules in a closed
875 metamorphic system (from Feneyrol et al. 2013). A- The sedimentary nodule is initially an
876 anhydrite concretion within the silica-rich shales. These shales contained V(-Cr)-rich clays
877 and organic matter. B- At the beginning of the prograde metamorphism, the host shales turned
878 into schists, and V(-Cr)-rich clays and organic matter transformed into respectively V(-Cr)-
879 rich micas and graphite. For the formation of tsavorite, Si and Al came from the schist, V and
880 Cr from the clays and/or organic matter, and Ca from the anhydrite following the equation:
881 $3\text{CaSO}_4 + 2\text{Al}^{3+} + 3\text{SiO}_2 + 6\text{H}_2\text{O} \rightarrow \text{Ca}_3\text{Al}_2(\text{SiO}_4)_3 + 6\text{O}_2 + 3\text{H}_2\text{S} + 6\text{H}^+$.
882 H_2S is trapped by the fluid inclusion cavities in tsavorite. The sulphur is expelled into the
883 schist to form pyrite. C- At the end of the prograde metamorphism, most of the anhydrite has
884 been replaced by tsavorite which is also present as small crystals scattered in the evaporitic
885 rims of the nodule. Pyrite, graphite and V(-Cr)-poor mica are the main minerals present in the
886 surrounding gneiss.

887

888 **Table caption**

889 **Table 1.** Reconstruction composition of emerald-related fluids from the Panjshir deposits,
890 Afghanistan (this work). For comparison are reported the composition of the fluids associated
891 with Colombian emeralds (Banks et al. 2000).

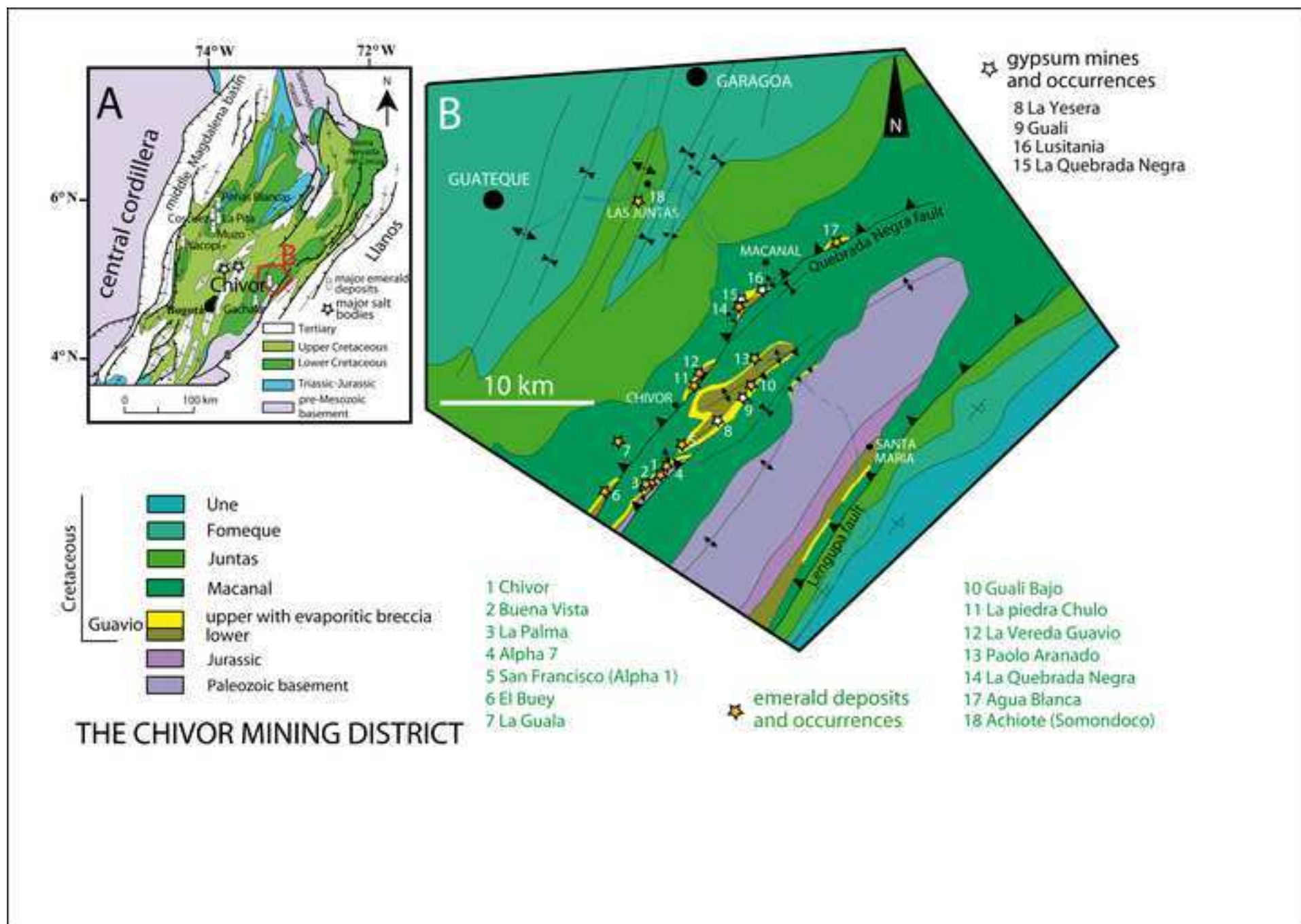
892

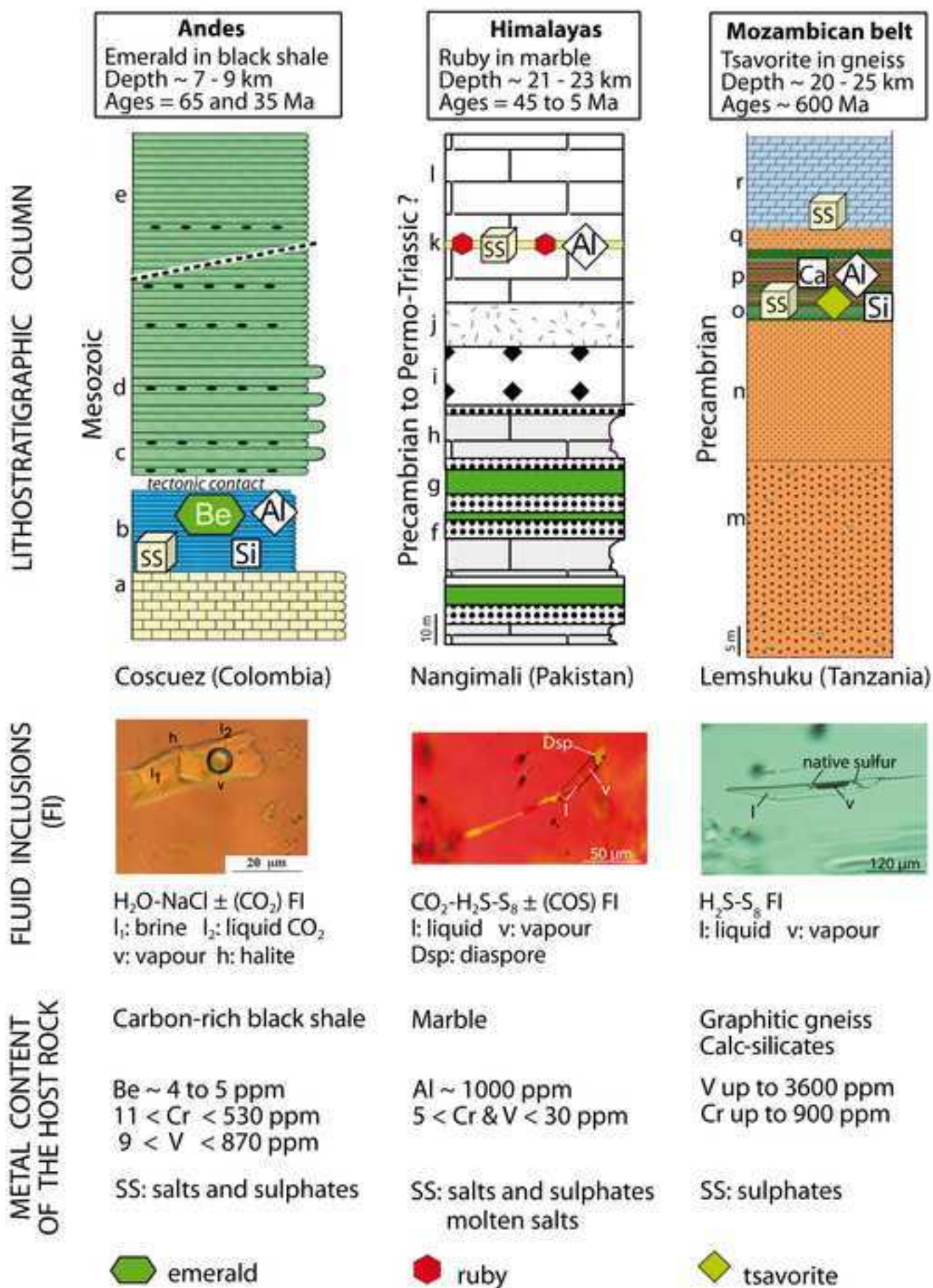
Table

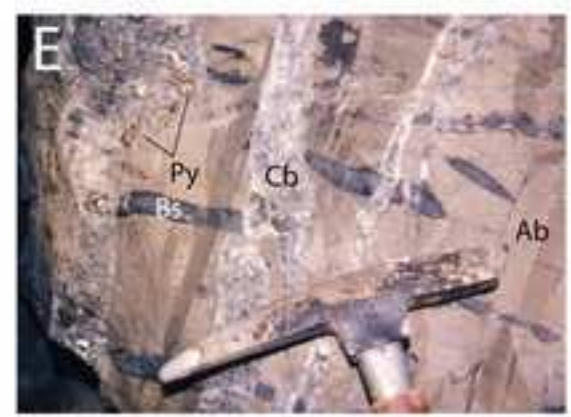
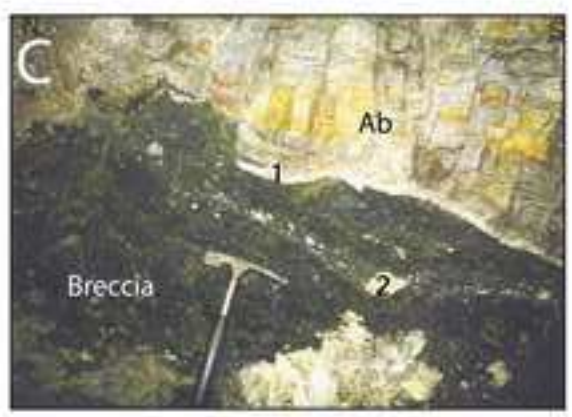
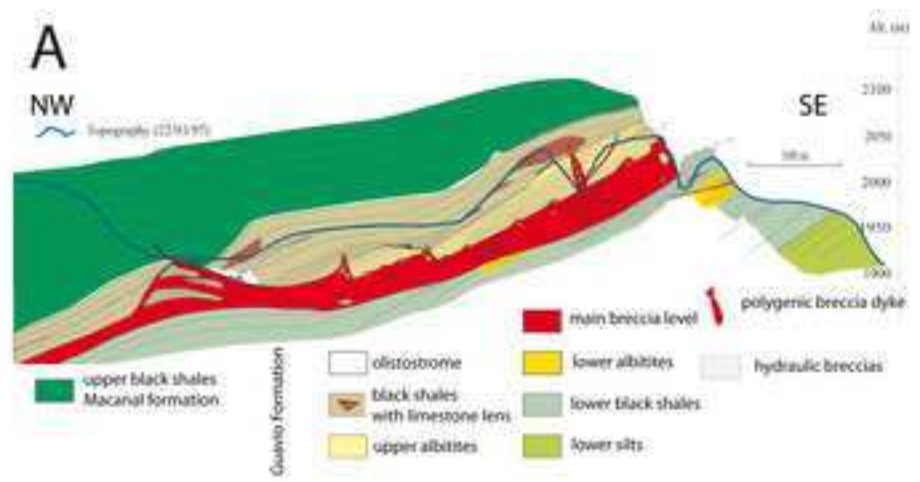
country	deposit	mineral	salinity (wt% eq. NaCl)	Na	K	Li	F (ppm)	Cl	Br	SO ₄	I	Na/K (m)	Na/Br (m)	Cl/Br (m)	Na/Li (m)	Cl/SO ₄ (m)	og(Br/Cl)log(I/Cl) (m)	
AFGHANISTAN																		
	Kendjt	quartz	34	103.711	25.250	171	118	206.310	44.2	147	0.29	6.98	8152.12	10520.63	182.55	3792.17	-4.02	-6.40
	Kendjt	"	34	107.729	26.800	180	115	206.310	36.4	143	0.31	6.83	10286.9	12780.53	180.24	3905.72	-4.11	-6.38
	Kendjt	emerald	34	78.205	34.062	207	670	206.310	41.4	4310	0.49	3.9	6563.65	11233.31	114.02	129.63	-4.05	-6.18
	Butizor	"	34	97.257	22.573	220	nd	206.310	20	1058	0.8	7.32	16928.4	23296.37	133.67	528.13	-4.37	-5.97
	Gujari	"	34	72.325	30.322	261	nd	206.310	39.8	1331	0.41	4.05	6311.74	11680.32	83.68	419.57	-4.07	-6.25
	Shigar	"	34	71.969	29.692	245	nd	206.310	41.2	824	0.52	4.12	6065.24	11279.71	88.73	677.63	-4.05	-6.16
COLOMBIA*																		
	Yacopi	emerald	38	100.376	22.585		nr	224.007	80.2	6491	4.5	7.56	4347.85	6294.79		93.45	-3.80	-5.25
	Coscuez	"	38	130.946	5795	944	nr	230.082	36.7	463	0.3	0.04	12395	14128.97	41.86	1345.61	-4.15	-6.44
	Cincho	"	37	94.823	18.813	1261	nr	224.306	39.7	166	1.9	8.57	8297.40	12733.39	22.69	3658.9	-4.10	-5.63
	Palo Aranado	"	40	122.677	8829	1165	nr	242.43	55.5	232	0.68	0.02	7678.72	9844.35	31.77	2829.55	-3.99	-6.11
	Oriente	"	38	116.142	5888	430	nr	230.202	27.4	352	0.36	0.03	14725.1	18934.43	81.5	1770.86	-4.28	-6.36
	Klein	"	40	98.923	10.248	1959	nr	240.698	51.0	1966	2.61	16.41	6738.23	10636.44	15.24	331.52	-4.03	-5.52
	Yacopi	quartz	40	94.019	19.556		nr	240.815	328.1	1567	0.9	8.17	995.47	1654.14		416.13	-3.22	-5.98
	Coscuez	"	35	54.590	11.622	2031	nr	211.091	100.6	1189	0.2	7.99	1885.10	4728.96	8.11	480.74	-3.67	-6.58
	Coscuez	"	41	106.484	14.833		nr	248.415	118.4	238	0.9	12.20	3124.29	4728.46		2826.31	-3.67	-5.99
	Coscuez	"	42	92.542	10.467	2212	nr	254.132	65.8	658	3	15.03	4885.76	8704.17	12.62	1045.81	-3.94	-5.48
	Cincho	"	39	63.557	11.567	4322	nr	230.481	99.0		1.6	9.34	2230.22	5246.79	4.44		-3.72	-5.71
	Cincho	"	41	103.599			nr	247.813	390	558	5		922.80	1432.03		1202.56	-3.16	-5.25
	Pava	"	41	110.776	5449	432	nr	227.371	150.7	24	2.7	0.03	2553.59	3400.29	77.37	25653.2	-3.53	-5.48
	Oriente	"	31	76.239	12.389		nr	188.233	87.7	997	3.1	10.46	3019.93	4837.15		511.23	-3.68	-5.34
	Klein	"	31	68.344	8796	2549	nr	183.208	42.8		1.5	0.01	5547.22	9647.05	8.09		-3.98	-5.64
	Guali	"	40	78.554	17.415	2090	nr	242.078	23.8	614	2.2	7.67	11466	22923.04	11.34	1067.59	-4.36	-5.60

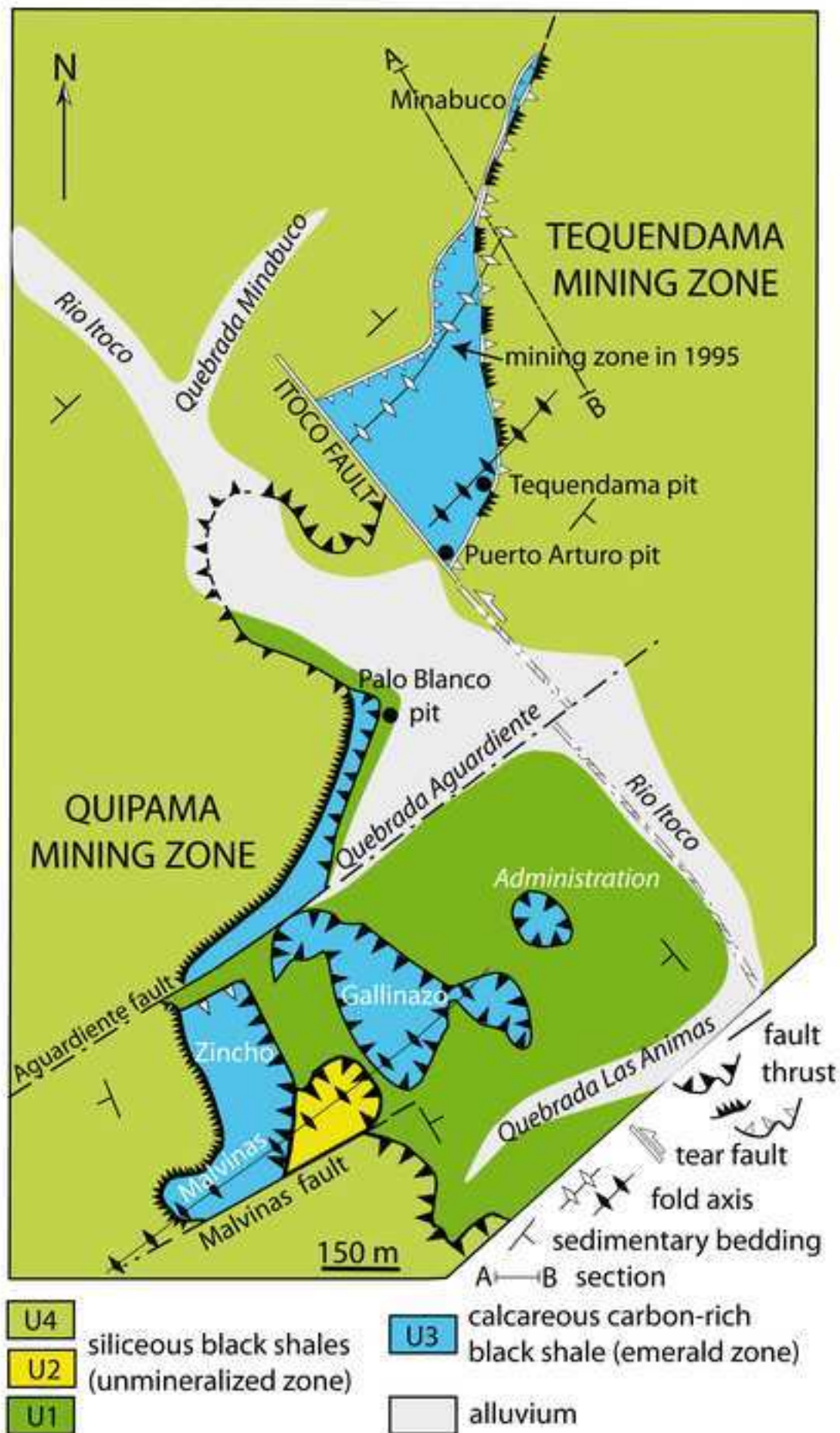
nd: not detected; nr: not reported because measured at the limit of detection (~ 1ppm); * Banks et al. (2000)

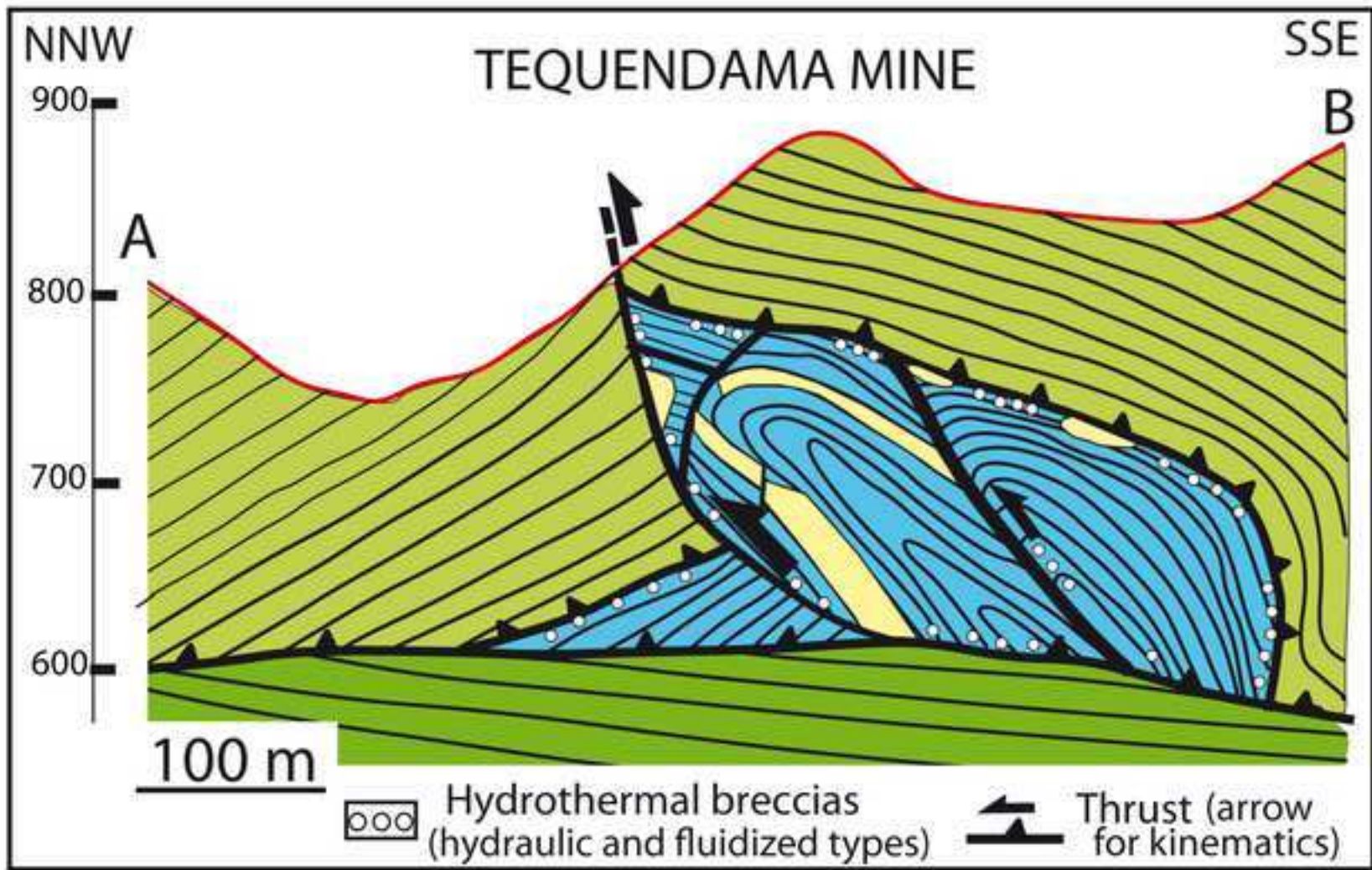






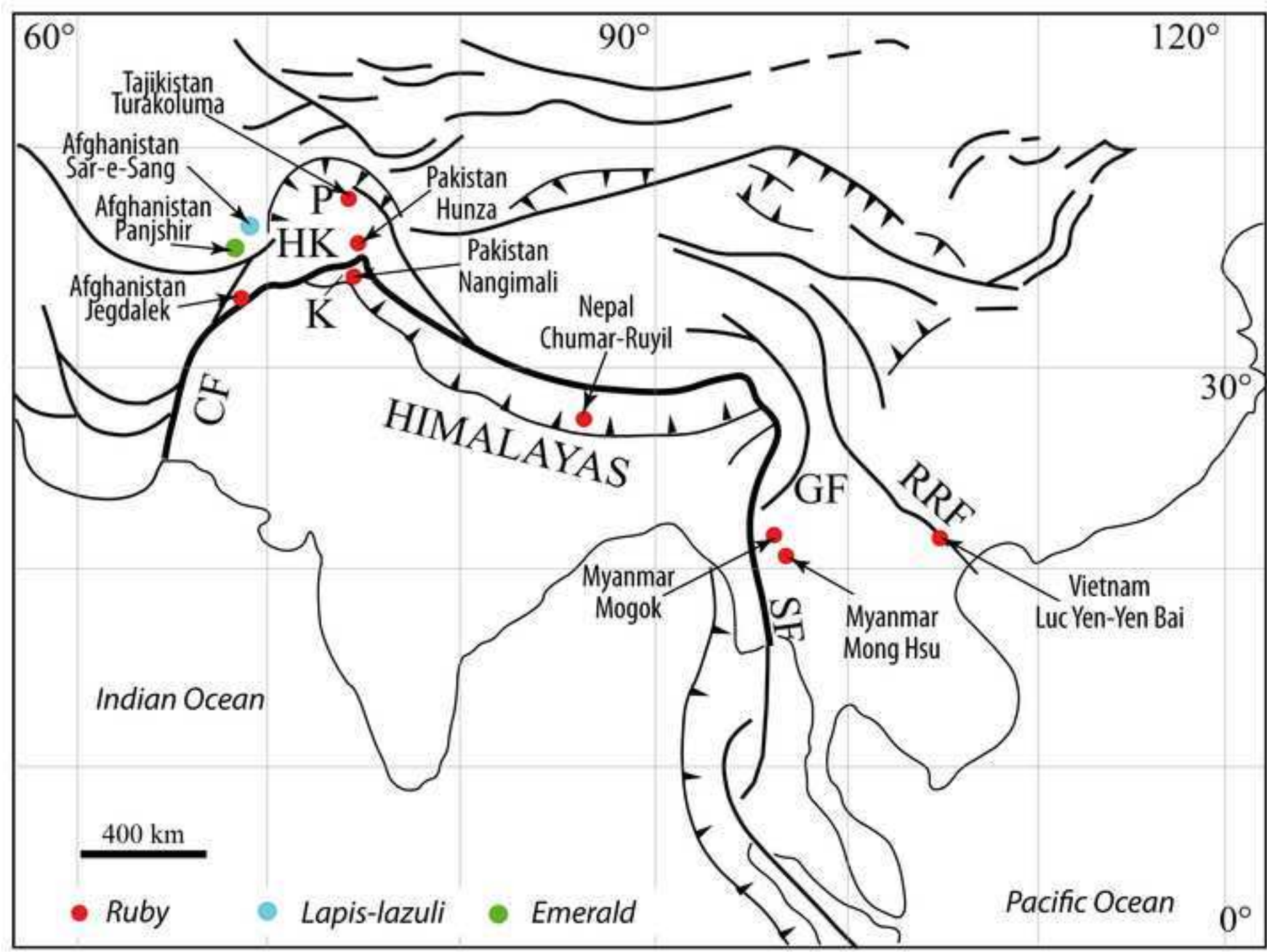


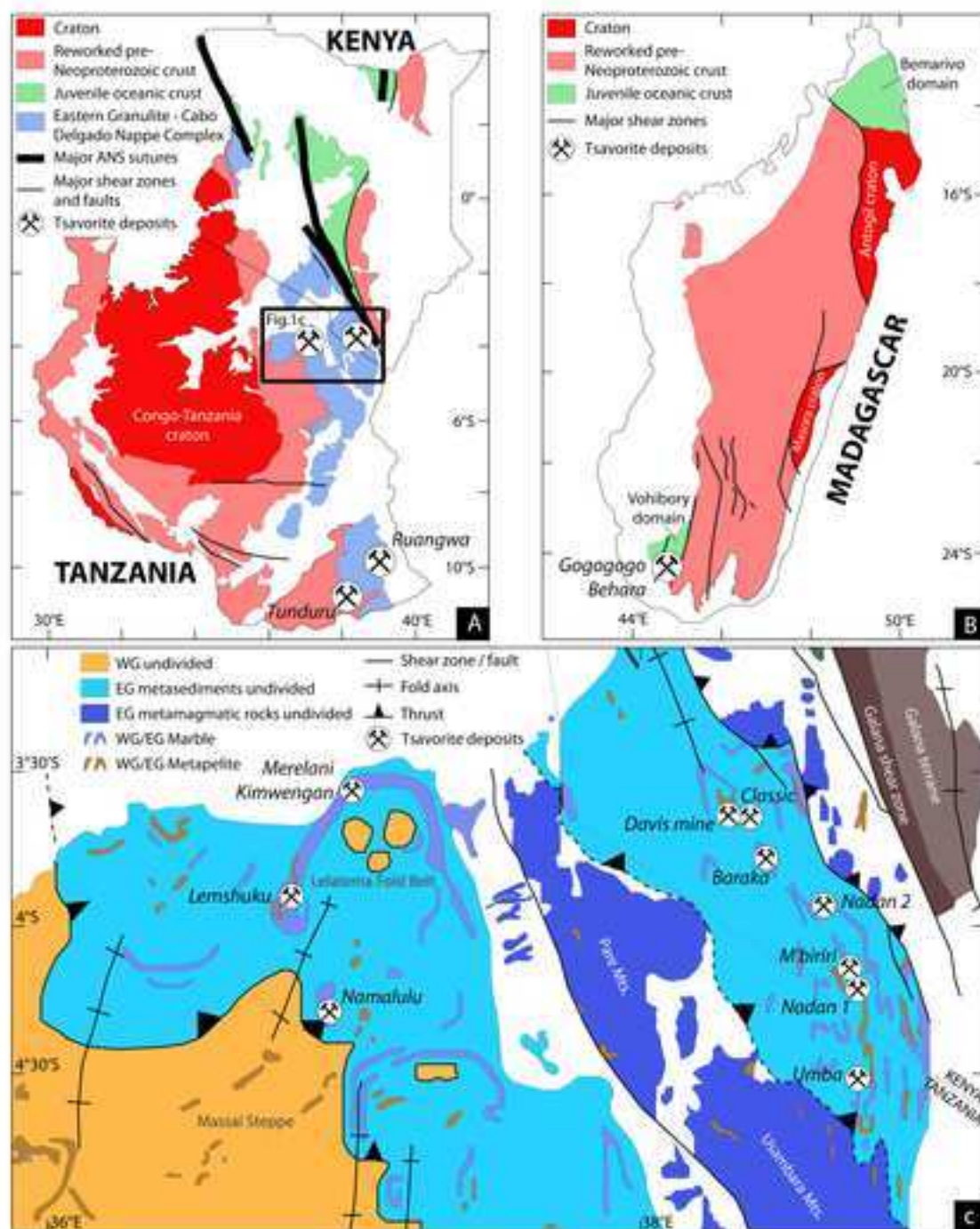


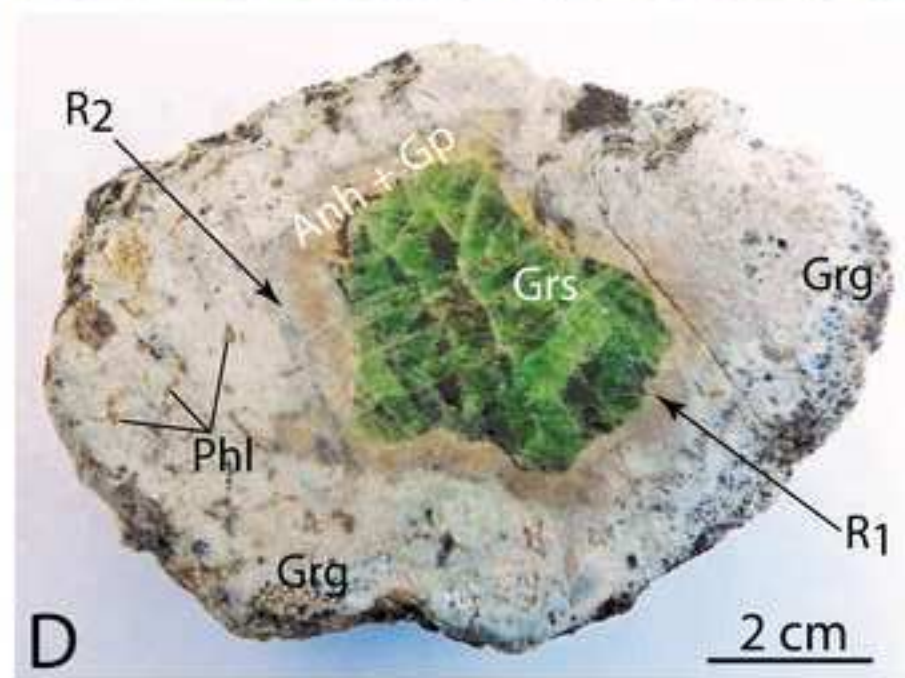
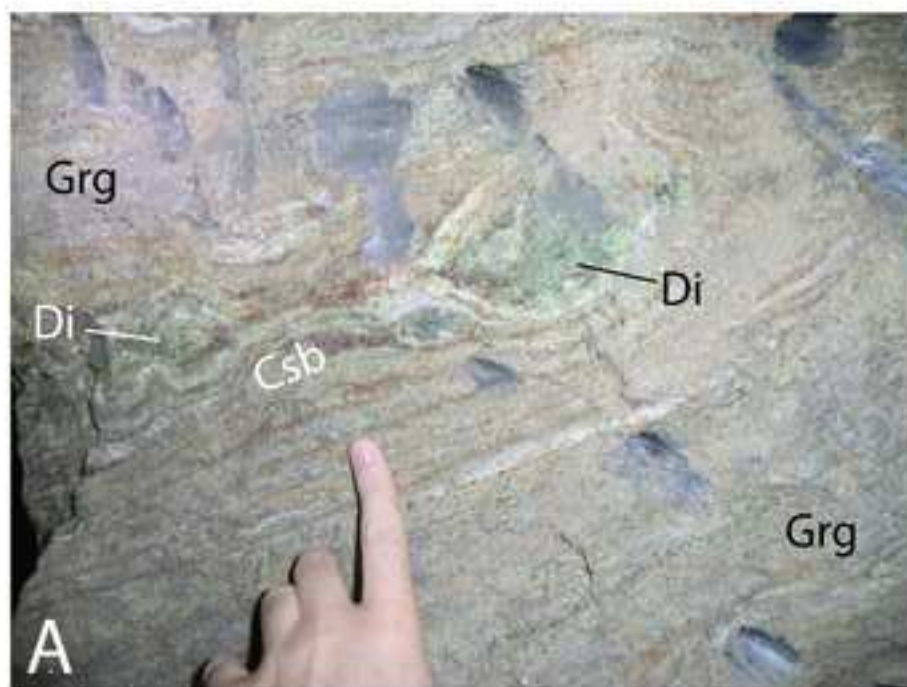


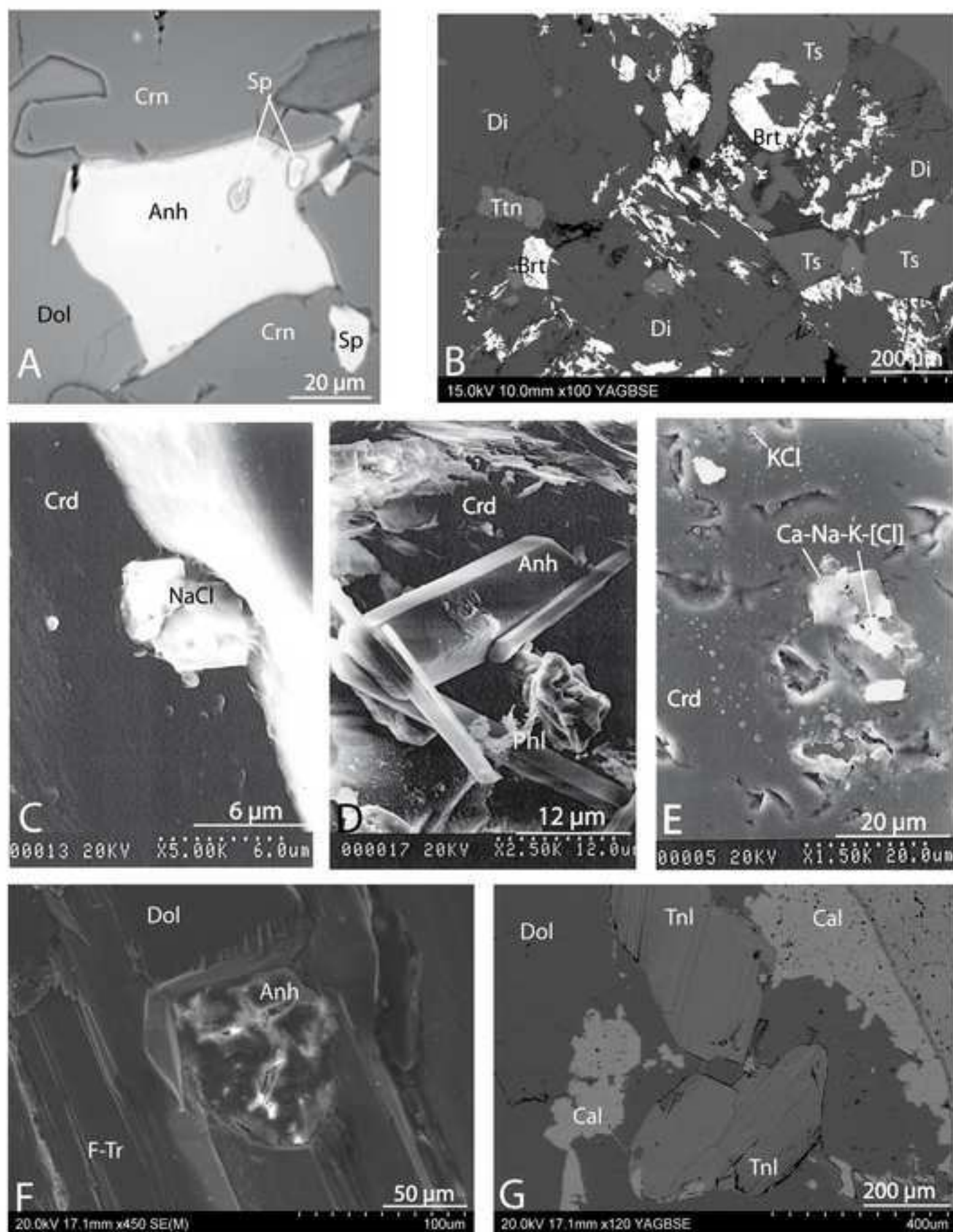
- ↑ siliceous black shales (permeability barrier)
- carbonated black shale (fluid-saturated rock mass)
- albitites

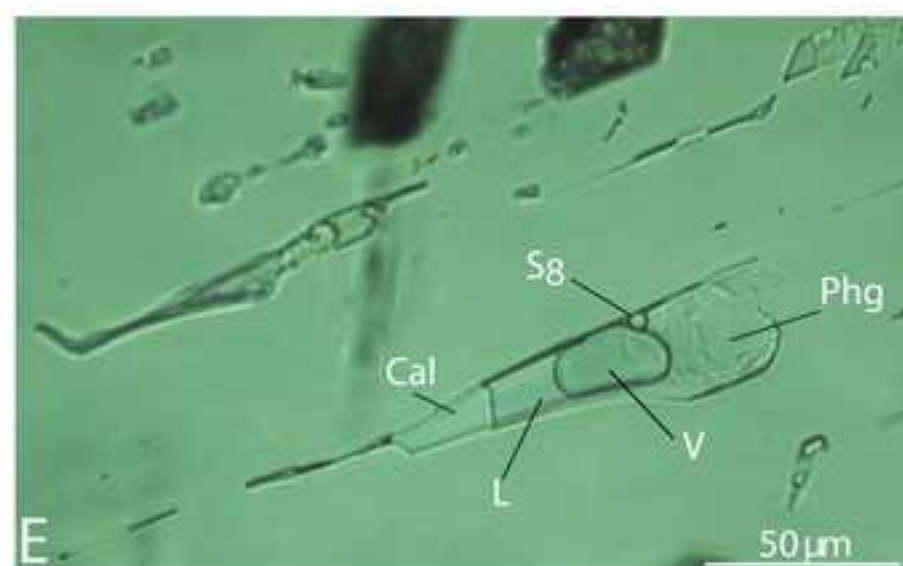
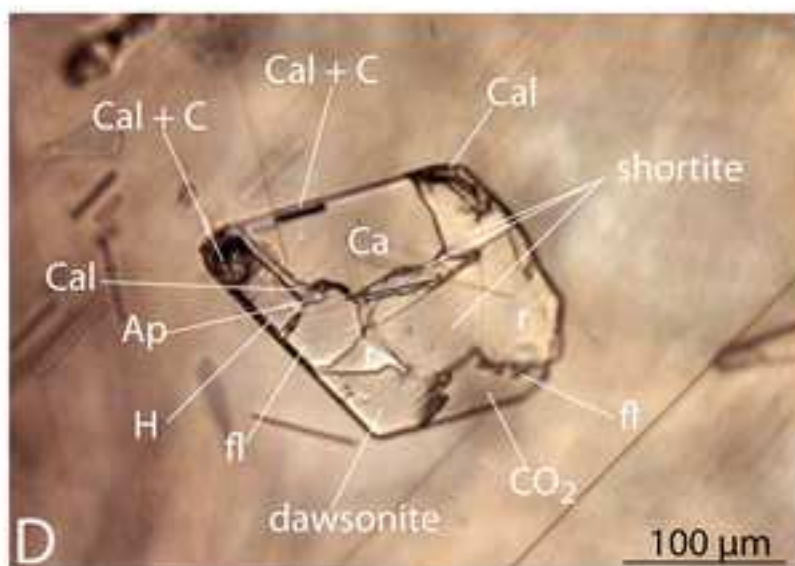
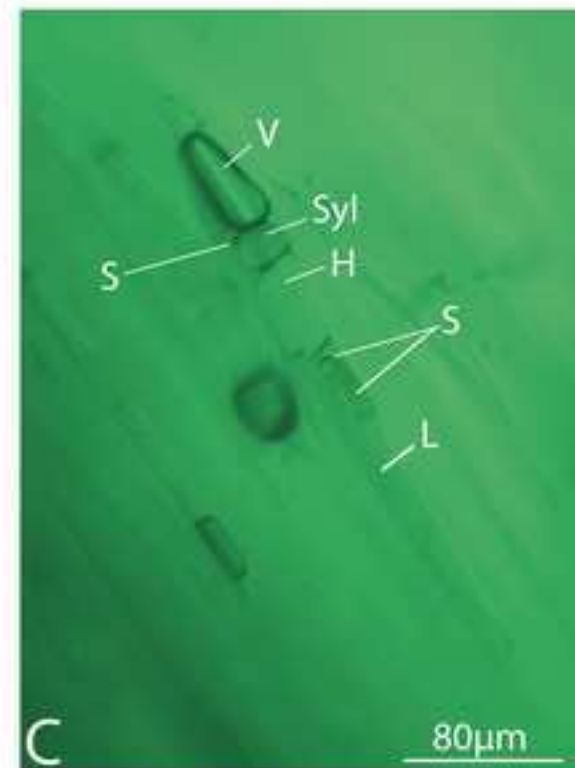
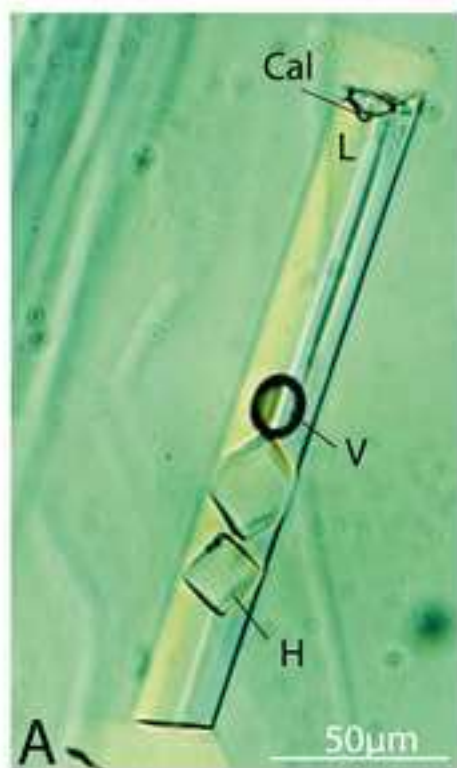


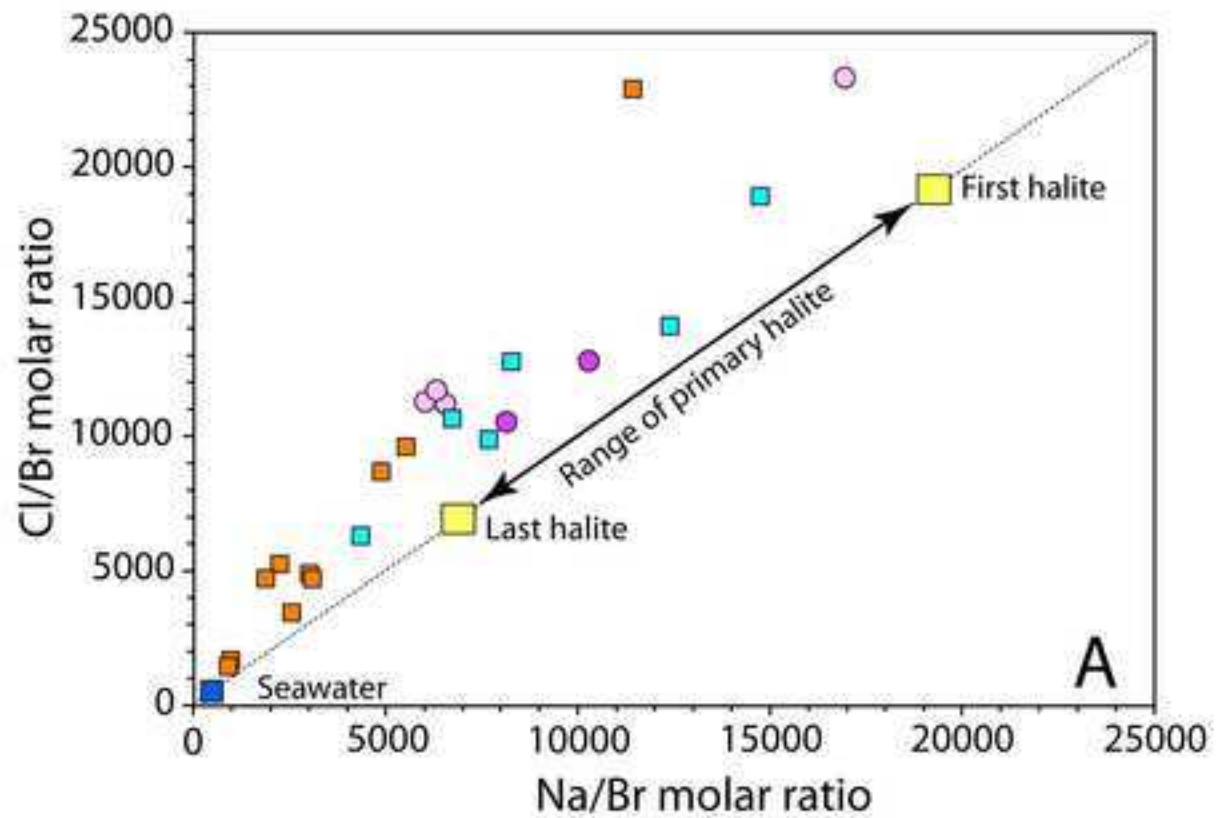












Afghanistan
● quartz
● emerald

Colombia
■ quartz
■ emerald

